Topographically Generated, Subinertial Flows within A Finite Length Canyon

S. E. ALLEN

Oceanography, Department of Earth and Ocean Sciences, University of British Columbia, Vancouver, British Columbia, Canada

ABSTRACT

The presence of a canyon cutting the continental shelf has been observed to enhance wind-driven upwelling. In particular, in the vicinity of Juan de Fuca Canyon at the mouth of the Juan de Fuca Strait, an eddy containing deep water (from a depth of approximately 450 m) has been documented. Strong upcanyon flows have been observed within numerous canyons including Astoria Canyon, which cuts the shelf offshore of the mouth of the Columbia River. The author develop a linear theory for wind-driven flow over an infinitesimally thin but finite length canyon to illustrate the basic mechanism. Two regimes are considered, the initial growing velocity field and a later steady velocity field. The flow toward the shore is enhanced by $O(10)$ by the presence of the canyon in a homogeneous fluid. The presence of stratification introduces smaller horizontal length scales, the baroclinic Rossby radius, and allows further enhancement of the upcanyon flow.

Numerical simulations show that the linear theory is a reasonable approximation for canyons of finite but narrow width compared with the baroclinic Rossby radius. The effect of nonlinearity is to advect the flow pattern downstream, which gives results closer to what is observed. In contrast to the case for linear flow, strong cyclonic vorticity is generated over the canyon, as is observed over Astoria Canyon.

1. Introduction

Freeland and Denman (1982) identified a region of upwelled California undercurrent water on the coastal shelf near the Juan de Fuca Canyon, which extends offshore across the shelf from Juan de Fuca Strait. The high nutrient content of this upwelled water is considered to be of importance to the productivity of nearby La Pérouse Bank (Mackas and Sefton 1982). Strong flows along the canyon axis have been observed within a number of canyons; examples include Quinault (Hickey et al. 1986), Hudson (Hotchkiss and Wunsch 1982), Lydonia and Oceanographer (Butman 1983), and Moresby Trough (Ma 1992). Extensive current meter observations, during upwelling favorable winds, have been made in Astoria Canyon, which cuts the shelf offshore from the Columbia River (B. Hickey 1996, submitted to *J. Phys. Oceanogr.*).

The presence of a cold water anomaly in the region of the Juan de Fuca Canyon is a persistent feature. Recent work, Fang and Hsieh (1993), has shown that an empirical orthogonal function (EOF) incorporating this feature (as well as shelf break upwelling) is the second EOF, and accounts for 12% of the variance, in summer sea surface temperature off Vancouver Island. The upwelled water is not upwelled to the sur-

face but is mixed so that its signature reaches the surface. The outflow of Juan de Fuca Strait is part of the first EOF.

Freeland and Denman (1982) proposed that the enhanced upwelling over Juan de Fuca Canyon is due to cross-shore pressure gradients that, within the canyon, the Coriolis force cannot balance. They showed, using an available energy argument, that such pressure gradients were capable of bringing water originally at 450 m onto the shelf. Klinck (1988, 1989) considered the adjustment of a jet crossing an infinitely long, flat-bottom canyon with vertical edges. The linear shallow water equations were solved for homogeneous and stratified flow. As the shelf was included in the model, the effect of upwelled water on the cross-shore pressure gradient was incorporated. This model showed that, if the canyon width is less than half the Rossby radius, the transverse flow is unimportant in the canyon. By this criterion the Tully Canyon, a spur of Juan de Fuca Canyon, which appears to be associated with the upwelling, is a narrow canyon as its width is approximately 7 km compared to the local baroclinic Rossby radius, which is approximately 17 km. Astoria Canyon, about 6 km wide with a similar Rossby radius, is even a narrower canyon. Recent numerical simulations using the Blumberg–Mellor model have been done over smoother canyon topography (Allen 1992). The advantage of the Blumberg–Mellor model is that it can handle continuous stratification. However, in order to consider steep slopes, a layered stratification will be used here.

Corresponding author address: Dr. Susan E. Allen, Oceanography, Department of Earth and Ocean Sciences, University of British Columbia, 6270 University Blvd., Vancouver, BC V6T 1Z4, Canada.

In this paper, the modeling of topographically generated flow within a canyon is extended to include 1) a finite length canyon with a head, ending on the shelf and a mouth, opening at the shelf break and 2) full consideration of the flow over the shelf, within the canyon and off the shelf break. Freeland and Denman (1982) included the former and not the latter of these, whereas Klinck (1989) included the latter and not the former. If the reduction in cross-shore pressure gradient due to upcanyon flow is included, a finite length canyon cannot support steady upcanyon flow without continuous (in time) forcing. The combination of 1) and 2) leads to a different theory of upcanyon flow.

In section 2 an infinitesimally thin canyon in a homogeneous fluid is considered. The canyon is of finite length, opening to the deep ocean at the shelf break and ending on the shelf. The geometry is illustrated in Fig. 1 and represents an extreme canyon, long and reasonably deep. Canyons that more closely represent Astoria and Tully will be considered in section 6. A steady upwelling favorable wind is assumed. The wind produces an Ekman layer (not modeled) whose effect on the main body of the fluid is modeled by a sink at the coast, in the manner of Pedlosky (1974). In section 3 we extend the theory to a three-layer stratified fluid.

As time increases the alongshore flow will reach a steady state where bottom friction balances the surface forcing. The steady-state theory is derived in section 4. In section 5 we compare the equilibrium analytic theory to a linear numerical model for a narrow but finite width canyon. In section 6 results are shown and discussed for nonlinear numerical simulations. The numerical models illustrate the adjustment to the equilibrium solution, which occurs through Poincaré, topographic Rossby, and in the case of stratified flow, baroclinic Kelvin waves. Two cases, one representing Tully Canyon and one representing Astoria Canyon, are compared qualitatively to some of the available field results. Effects due to variations in the stratification, geometry, and forcing are considered. The last section gives a summary and some concluding remarks.

2. Acceleration phase

The acceleration phase describes the flow characteristics in the one-half to three day time period after the wind becomes upwelling favorable; that is, there is offshore Ekman transport in an upper Ekman layer. The Ekman layer (not modeled) must be "fed" at the coast, and thus the effect of the wind stress is to produce a sink for the main body of fluid at the coast.

The above assumptions inherently assume the upper Ekman layer is thin compared with the full depth of the fluid. This assumption is valid near the shelf break for both Astoria and Tully and neither of these canyons closely approach the coast. For consistency, the coast is assumed vertical. These assumptions lead to a wind-driven current that lies closer to the coast than is ob-
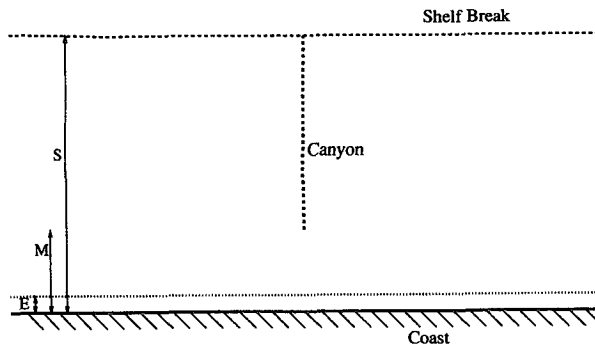

FIG. 1. A plan view of the model geometry. The canyon is flat along its length, infinitesimally thin (very thin for the numerical work). The forcing width is $E = 0.05a$; the margin width is $M = 0.2a$, and the shelf width is $S = 2a$, where a is the barotropic Rossby radius. The canyon is 400 m deep and cuts through a shelf 50 m deep. The shelf break is a step.

served. The position of the current can be adjusted in the theory by varying the parameter E the distance from the shore over which the Ekman sink acts.

As the forcing consists of removal of fluid at a constant rate, the total amount of fluid removed will increase linearly with time. We shall look for a two-part equilibrium solution in which one part increases linearly with time and the other is constant in time. Such a solution excludes waves (topographic and gravity) and inertial oscillations. It is the solution expected after the waves have propagated away leaving an equilibrium solution. The waves are included in the numerical solutions and it will be shown in section 6 that they do propagate quickly enough for this equilibrium solution to be realized.

The linear barotropic shallow water equations, excluding the surface Ekman layer, are

$$\frac{\partial \mathbf{u}}{\partial t} + f\mathbf{k} \times \mathbf{u} = -g\nabla\eta \qquad (1a)$$

and

$$\frac{\partial \eta}{\partial t} + \nabla \cdot (h\mathbf{u}) = -q, \qquad (1b)$$

where η is the surface height, $\mathbf{u} = (u, v)$ is the horizontal velocity, g is the acceleration due to gravity, f is the Coriolis frequency, h is the fluid depth, and $\mathbf{k}$ is the vertical unit vector. The x axis is taken to lie along the coast and the y axis along the axis of the canyon so that y increases offshore. The Ekman pumping at the coast is

$$q = \begin{cases} q_0, & y < E \\ 0, & y > E, \end{cases} \qquad (2)$$

where $q_0 = \tau/Ef$ to match the flux in the Ekman layer and τ is the steady and uniform wind stress, assumed

to be in the alongshore direction. From the shallow water equations a potential vorticity conservation equation can also be derived:

$$\frac{\partial}{\partial t}(h\nabla \times \mathbf{u} - f\eta) = f\mathbf{u}\cdot\nabla h + fq. \qquad (3)$$

We let $\eta = \eta_1 ft + \eta_0$, $u = u_1 ft + u_0$, and $v = v_1 ft + v_0$. Substitution gives the following equations proportional to t:

$$f\mathbf{k}\times\mathbf{u}_1 = -g\nabla\eta_1 \qquad (4a)$$

and

$$\nabla\cdot(h\mathbf{u}_1) = 0. \qquad (4b)$$

We note that (4a) implies (4b) over flat topography and together they imply that there is no growing velocity field (u_1, v_1) parallel to the depth gradient. That part of (1) constant in time gives

$$f\mathbf{u}_1 + f\mathbf{k}\times\mathbf{u}_0 = -g\nabla\eta_0 \qquad (5a)$$

and

$$f\eta_1 + \nabla\cdot(h\mathbf{u}_0) = -q. \qquad (5b)$$

At this point, it is useful to separate the steady velocity into that part in geostrophic balance with the constant surface elevation,

$$f\mathbf{k}\times\mathbf{u}_c = -g\nabla\eta_0 \qquad (6)$$

and that part in balance with the growing velocity field,

$$f\mathbf{u}_1 + f\mathbf{k}\times\mathbf{u}_s = 0. \qquad (7)$$

The steady momentum equation (7) implies that, in the absence of a constant surface elevation η_0 for a linearly increasing (in time) velocity field, there must be a corresponding steady velocity field perpendicular to it to accelerate the growing velocity in regions beyond the forcing. Alternatively, one can consider the steady velocity to be necessary to move fluid down the pressure gradient (the growing velocity is perpendicular to it) to feed the Ekman layer at the coast. The velocities $\mathbf{u}_1$ and $\mathbf{u}_c$ are geostrophic, whereas $\mathbf{u}_s$ is the ageostrophic velocity. Substituting the assumed form of the solution into the potential vorticity equation gives

$$h\nabla\times\mathbf{u}_1 - f\eta_1 = \mathbf{u}_0\cdot\nabla h + q. \qquad (8)$$

Away from topographic changes, the equations for η_1, (4a) and (8), reduce to the equation

$$a^2\nabla^2\eta_1 - \eta_1 = \frac{q}{f}, \qquad (9)$$

and for η_0 the integral of (3), (4b), and (5) and assuming the flow starts from rest, reduce to the equation

$$a^2\nabla^2\eta_0 - \eta_0 = 0, \qquad (10)$$

where $a = \sqrt{gh}/f$ is the local, barotropic Rossby radius.

a. Primary circulation

The primary circulation [a solution of (9)] consists of the velocity $\mathbf{u}_1$ that grows in time, the steady velocity $\mathbf{u}_s$ in balance with it, and the growing surface elevation η_1. The secondary circulation [a solution of (10)] consists of the steady surface elevation η_0 and the steady velocity $\mathbf{u}_c$. The benefit of this seemingly arbitrary separation is that the primary circulation satisfies the boundary conditions at the coast and at the canyon. The secondary circulation is only required to satisfy the steady flux conditions at the shelf. The boundary conditions for a ridge (the divergence of the steady flux must be zero) do require a steady surface deflection, and this is where the solution for a ridge and a canyon diverge.

For clarity, at this point we nondimensionalize all horizontal length scales by a_s, the Rossby radius over the shelf.

The boundary conditions for the primary circulation problem must be written in terms of η_1 to use with (9). At the coast, $y = 0$, the normal velocity must be zero. Thus, v_1 is zero and therefore by (4a), $\partial\eta_1/\partial x$ is zero and the value of η_1 is uniform along the wall. The response is expected to be trapped to the coast, so the surface elevation must approach zero far from the coast ($\eta_1 \rightarrow 0$ as $y \rightarrow \infty$). Along the shelf break, $y = S$, $\partial h/\partial y$ is not zero; so, as derived above, v_1 is zero and $\partial\eta_1/\partial x$ is zero. The growing surface height over the shelf break is uniform, η_s. In the absence of a canyon or well away from the canyon, $|x| \gg a_s$, the solution must be independent of x and these boundary conditions are sufficient. In this case, the solution has the form of the standard Rossby adjustment problem near a coast, modified by the presence of the shelf break. The solution is given in the appendix and will be denoted $\bar{\eta}_1$.

Now consider the vicinity of the canyon. The surface height over the shelf break is given by the value far from the canyon; that is, from the solution in the absence of a canyon,

$$\eta_s = -\sigma\frac{q_0}{f}\sinh E\, e^{-S}. \qquad (11)$$

See the appendix for the derivation and definition of σ. Over the canyon side walls $\partial h/\partial x$ is not zero, so u_1 is zero and, thus, $\partial\eta_1/\partial y$ must be zero. The value of surface height over the canyon walls is given by the value over the shelf break, η_s. With the boundary condition at the wall, the boundary condition as $y \rightarrow \infty$, and the expectation that the perturbation due to the canyon will be trapped, the conditions along the shelf break and canyon give a full set of boundary conditions. However, we need only solve for the solution in the first quadrant and invoke symmetry. For a linear solution, there should be a line of symmetry through the center of the canyon so that between the canyon and the wall, $\partial\eta_1/\partial x = v_1 = 0$.

The solution in the absence of a canyon is a particular solution of (9) and a homogeneous solution must be found to satisfy the boundary conditions at the canyon wall. If we remove the particular solution and define the homogeneous solution as

$$\phi = \eta_1 - \bar{\eta}_1(y), \tag{12}$$

then ϕ satisfies the homogeneous equation,

$$\nabla^2\phi - \phi = 0 \tag{13}$$

with boundary conditions:

$$\phi = 0, \quad \text{at} \quad y = 0, S \tag{14a}$$

$$\phi \to 0, \quad \text{as} \quad x \to \infty \tag{14b}$$

$$\frac{\partial\phi}{\partial x} = 0, \quad \text{at} \quad x = 0, \quad y = [0, M] \tag{14c}$$

and

$$\phi = \eta_s - \bar{\eta}_1(y), \quad \text{at} \quad x = 0, \quad y = [M, S], \tag{14d}$$

where $y = M$ is the near-coast end of the canyon. The general solution satisfying the boundary conditions at $y = 0$ and $y = S$ is given by the Fourier sum,

$$\phi = \sum_{n=1}^{\infty} A_n(x) \sin\left(\frac{n\pi y}{S}\right). \tag{15}$$

Substituting into (13) gives

$$A_n(x) = c_n \exp\left\{-x\left[1 + \left(\frac{n\pi}{S}\right)^2\right]^{1/2}\right\}, \tag{16}$$

where the second solution has been rejected on the basis of the boundary conditions as $x \to \infty$. The constants c_n are constrained by the boundary conditions at $x = 0$ (14c,d). If the Fourier series is truncated at some large number of modes, N, the c_n are found by inverting an $N \times N$ matrix. The solution for the extreme model canyon case $S = 2.0$, $M = 0.2$, $E = 0.05$ is given in Fig. 2 using $N = 50$. The size of N is determined by the resolution needed between the end of the canyon and the wall. With $M/S = 0.1$, at least $N = 20$ is needed and $N = 50$ gives a smoother solution.

The other fields can be found from the solution for η_1. As the divergence of the (u_1, v_1) flow is zero, the surface height also serves as the streamfunction for the growing velocity. The ageostrophic part of the steady velocity (u_s, v_s) can be found from the increasing velocity, (u_1, v_1), by using (5). This steady velocity is everywhere perpendicular but proportional to the increasing velocity.

At the canyon the surface height is continuous but not smooth. Thus, the (u_0, v_0) field shows strong divergence over the canyon. This divergence must be supplied by fluid flowing up through the canyon, which implies upcanyon flow consistent with upwelling.
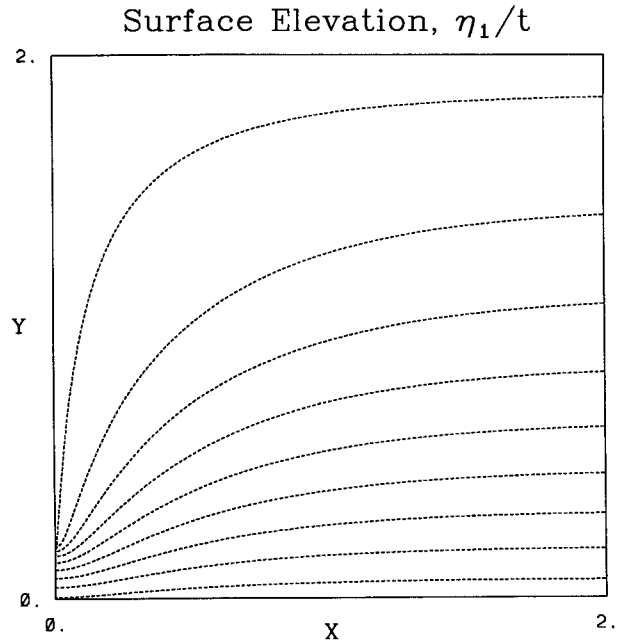
Surface Elevation, η_1/t

FIG. 2. The growing surface elevation η_1 for the model geometry of Fig. 1. The canyon lies along $x = 0$ and the coast is at $y = 0$. Contoured from 0.1 to 0.9 by 0.1 of η_s.

The velocity over the canyon walls, u_s, is $-v_1$ and the total flux per unit length out of the canyon is $2u_s h = -2v_1 h$, where by (4a) $v_1 = (g/f)\,\partial/\partial x$ of (15). Integrating the flux, $2u_s h$ over the length of the canyon, $y = [M, S]$ gives the total flux through the canyon at $y = S$, which in dimensional variables is

$$F = \lambda q_0 \sinh(E/a_s)a_s^2 = -2Sfa_s$$

$$\times \sum_{n=1}^{N} \frac{c_n}{\pi n}\left[1 + \left(\frac{n\pi a_s}{S}\right)^2\right]^{1/2}$$

$$\times \left[(-1)^n - \cos\left(\frac{n\pi M}{S}\right)\right]. \tag{17}$$

The value of λ varies from about 0.5 to 3 depending on the sizes of S/a_s and M/a_s. Figure 3 gives the value of λ as a function of M/S for various S/a_s. The flux at the shelf break in the absence of a canyon, over a width C, is $v_0 h$, which is (again in dimensional variables)

$$a_d C \frac{q_0 \sinh(E/a_s)}{\sinh(S/a_s) + 1/\alpha \cosh(S/a_s)}, \tag{18}$$

where $\alpha = \sqrt{H_S/H_D}$ and a_d is the barotropic Rossby radius off the shelf.

The ratio of these is

$$\lambda \frac{a_s}{C}[\alpha \sinh(S/a_s) + \cosh(S/a_s)]. \tag{19}$$
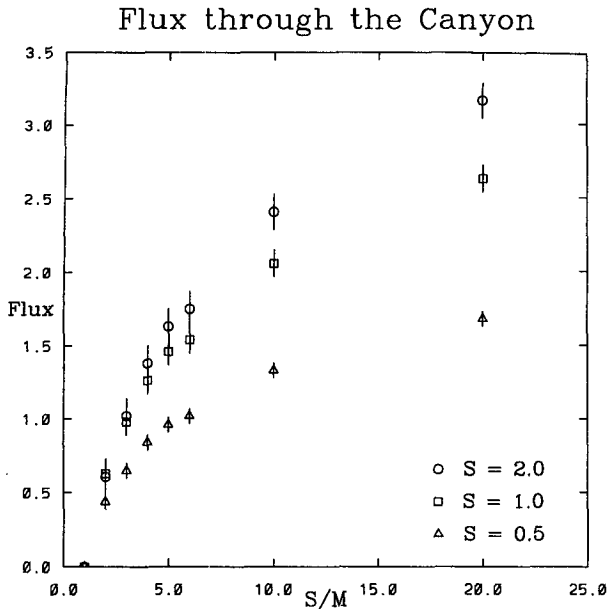
Flux through the Canyon

FIG. 3. The total flux through the canyon divided by $q \sinh(E/a_s)$ as a function of the shelf width over the margin width S/M for various values of the shelf width S. The error bars reflect the level of approximation inherent in approximating the sum, (17), by 100 terms. The forcing width is $E = 0.05a_s$.

This ratio is a measure of the enhancement of upwelling due to the canyon.[1] For a finite width canyon, C should be taken as the canyon width. For the approximate dimension of Tully Canyon, that is, for a shelf of width 90 km with a canyon 8 km wide cutting to within 45 km of the coast with a shelf depth of 100 m and an offshelf and canyon depth of 250 m, the ratio is 13.

b. Secondary circulation

In the absence of a canyon, the flow off the shelf is that given in the appendix and consists of a growing surface height perturbation, a growing alongshore velocity and a steady upwelling flux toward the shore. The flow across the shelf from deep water matches that on the shelf. The boundary conditions for the steady surface height η_0 are zero (wall, shelf break, far from the coast) and thus by (10), $\eta_0 \equiv 0$.

However, in the case with a canyon, the steady flux $v_s h$ does not match across the shelf break and a steady surface elevation field and its accompanying geostrophic velocity v_c is required to close the problem. The presence of the canyon causes two changes in the flux pattern. First, in the vicinity of the canyon the onshore flux across the shelf break is reduced and this flux is redirected through the canyon instead. Second, there is an additional flux that goes through the canyon to maintain the higher surface heights in the vicinity of the canyon than would be present is its absence.

To support this change in flux across the shelf break in the vicinity of the canyon, a steady η_0 field must be present. This field is steady as the growing surface elevation height along the shelf break is unaffected by the canyon. But a steady η_0 field over the deep ocean implies a steady η_0 field over the shelf. The boundary conditions that must be satisfied at the shelf break are conservation of flux: $h(\partial \eta_1/\partial y - \partial \eta_0/\partial x)$ continuous, and continuity of pressure: η_0 continuous. Thus, over the shelf break we have, in dimensional variables,

$$\frac{\partial \eta_0}{\partial x} = -\frac{H_S}{H_D - H_S}\frac{\partial \eta_1}{\partial y} + \delta(x)\frac{fF}{g(H_D - H_S)}, \quad (20)$$

where F is the total flux up the canyon given by (17). The flux up the canyon implies a step change in η_0 across the canyon and, because part of the flux is not compensated by a decrease over the shelf break, there must be a net step change between $x \to -\infty$ and $x \to \infty$. As shelf waves travel with the coast on the right we expect that to the left, far from the canyon, the surface height is unchanged. Thus, $\eta_0 = 0$ as $x \to -\infty$. Inserting the expansion for η_1 and integrating (20) from $x \to -\infty$ gives

$$\eta_s = \eta_0(y = S)$$

$$= -\frac{H_S}{H_D - H_S}\frac{\pi}{S}\sum \frac{c_n(-1)^n n}{\omega_n}\exp(\omega_n x), \, x < 0$$

$$= \frac{H_S}{H_D - H_S}\left[\frac{\lambda q_0 \sinh(E)}{f} - \frac{\pi}{S}\sum\frac{c_n(-1)^n n}{\omega_n}\right.$$

$$\left. \times (1 - \exp(-\omega_n x))\right], x > 0 \quad (21)$$

at the shelf break $y = S$ and where all the horizontal length scales have been made nondimensional by a_s and with $\omega_n = \sqrt{1 + (\pi n/S)^2}$. The other boundary conditions are surface elevation zero at the wall ($\eta_0 = 0$ at $y = 0$) and over the canyon ($\eta_0 = 0$ at $x = 0$ and $y = [M, S]$) and far from the coast ($\eta_0 \to 0$ for $y \to \infty$). The shelf break divides the region of solution into two.

On the ocean side of the shelf break the solution can be found using an infinite Fourier transform in the method of Gill et al. (1986). Transforming (10) with respect to x gives the Fourier transform of η_0 as the product of the Fourier transform of the value of η_0 at $y = S$ and of

$$\exp[(-y + S)(\alpha^2 + \kappa^2)^{1/2}], \quad (22)$$

where the other solution has been rejected on the basis of the boundary conditions for y large. By the convolution theorem,

$$\eta_0 = \frac{\alpha(y - S)}{2\pi}\int_{-\infty}^{\infty}$$

$$\times d\xi \frac{\mathcal{K}_1\{\alpha[(y - S)^2 + \xi^2]^{1/2}\}}{[(y - S)^2 + \xi^2]^{1/2}}\eta_s(x - \xi), \quad (23)$$

where $\mathcal{K}_1$ is a modified Bessel function; see Abramowitz and Stegun (1972).

Over the shelf the problem is complicated by the boundary conditions at the canyon. The height along the shelf break (21) can be separated into the exponential variation, which is purely odd in x, and a step change. The total solution is that due to the first part plus that due to the second.

The odd part automatically solves the boundary conditions at the canyon ($x = 0$). The solution for this part follows that above except the boundary conditions at $y = 0$ give the y part of the Fourier transform as

$$\frac{\sinh[y(1 + \kappa^2)^{1/2}]}{\sinh[S(1 + \kappa^2)^{1/2}]} . \tag{24}$$

The Fourier transform of this function can be found by conversion to exponentials and expansion of the denominator using a binomial expansion (valid for all S positive). Thus, this part of the solution over the shelf is

$$\eta_0 = \sum_{j=0}^{\infty} \frac{(y - (2j + 1)S)}{2\pi}$$

$$\times \int_{-\infty}^{\infty} d\xi \frac{\mathcal{K}_1\langle\{[y - (2j + 1)S]^2 + \xi^2\}^{1/2}\rangle}{\{[y - (2j + 1)S]^2 + \xi^2\}^{1/2}}$$

$$\times \eta_{s0}(x - \xi) - \sum_{j=0}^{\infty} \frac{(-y - (2j + 1)S)}{2\pi}$$

$$\times \int_{-\infty}^{\infty} d\xi \frac{\mathcal{K}_1\langle\{[-y - (2j + 1)S]^2 + \xi^2\}^{1/2}\rangle}{\{[-y - (2j + 1)S]^2 + \xi^2\}^{1/2}}$$

$$\times \eta_{s0}(x - \xi) \tag{25}$$

Each successive term in each sum is smaller by more than $\exp(-2S)$. Provided $S < 1.1$, only the first term in each sum is required to give a solution to better than 10%. For $S = 2$, the first term of the first series is sufficient.

The other part of the solution over the shelf is that due to the step change in η_s across $x = 0$. A solution of (10) that has the appropriate step change in η_s is zero at the wall $y = 0$, and approaches the expected far field solutions for x large is

$$\eta_0 = \sigma_3 \frac{\sinh y}{\sinh S}$$

$$+ \sum_{i=1}^{\infty} a_n \exp(-\omega_i x) \sin(i\pi y/S), \quad x > 0$$

$$= \sum_{i=1}^{\infty} b_n \exp(\omega_i x) \sin(i\pi y/S), \quad x < 0, \tag{26}$$

where σ_3 is the step part of η_s. The a_i and b_i are found in the way as for the growing solution η_1 with boundary conditions along $x = 0$. For $y < S$ the solution on the two sides must be equal and smooth; for $y > S$ the solution must be zero.

The secondary circulation for the extreme model canyon is given in Fig. 4.

The primary plus the secondary flux after 5 inertial periods for $S = 2.0$, $M = 0.2$, and a depth ratio of 8 is illustrated in Fig. 5.

3. Baroclinicity

To illustrate the effects of baroclinicity both on and off the shelf, a three-layer fluid is considered where the top two layer lie over the shelf but the lowest layer is deep enough only to occur off the shelf and within the canyon. A sketch of the configuration is given in Fig. 6. The governing equations are the linear shallow water equations:

$$\frac{\partial \mathbf{u}_u}{\partial t} + f\mathbf{k} \times \mathbf{u}_u = -g\nabla\eta \tag{27a}$$

$$\frac{\partial \eta}{\partial t} + h_u \nabla \cdot \mathbf{u}_u = -q \tag{27b}$$

$$\frac{\partial \mathbf{u}_m}{\partial t} + f\mathbf{k} \times \mathbf{u}_m = -g\nabla\eta - g'^1\nabla\xi' \tag{27c}$$

$$\frac{\partial \xi'}{\partial t} - \frac{\partial \eta}{\partial t} + \nabla \cdot (h_m \mathbf{u}_m) = 0, \tag{27d}$$

and off the shelf the above equations and

$$\frac{\partial \mathbf{u}_l}{\partial t} + f\mathbf{k} \times \mathbf{u}_l = -g\nabla\eta - g'^1\nabla\xi' - g'^2\nabla\xi'', \tag{27e}$$

$$\frac{\partial \xi''}{\partial t} - \frac{\partial \xi'}{\partial t} + \nabla \cdot (h_l \mathbf{u}_l) = 0, \tag{27f}$$

where ξ is the interface elevation; $\mathbf{u} = (u, v)$ is the horizontal velocity; $\mathbf{k}$ is the vertical unit vector; the subscripts u, m, l refer to the upper, middle, and lower layer respectively; the superscripts I and II refer to the interface between the upper and middle layer and the middle and lower layer respectively, and g'^1 and g'^2 are the reduced gravities across the I and II interfaces respectively. The reduced gravity is defined as $g\Delta\rho/\rho_0$, where $\Delta\rho$ is the density difference across the interface and ρ_0 is a reference density. Three equations, which express conservation of the potential vorticity for each of the three layers, can be derived in a fashion similar to the homogeneous case. Only the primary solution will be considered for the baroclinic case. Substituting a time-dependent part and a constant part, as was done for the homogeneous fluid, and through similar manipulation gives the following differential equations. On the shelf:

$$(R^2\nabla^2 - 1)(a^2\nabla^2 - 1)\eta_1 = -q \tag{28a}$$

$$(R^2\nabla^2 - 1)(a^2\nabla^2 - 1)\xi'_1 = 0, \tag{28b}$$
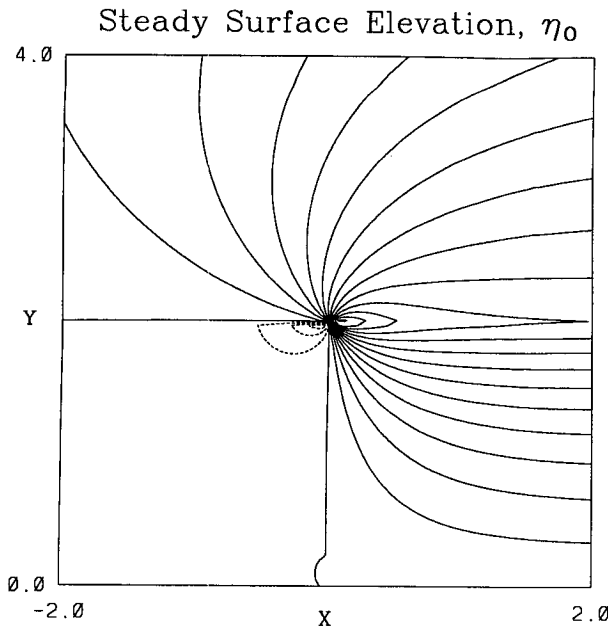
Steady Surface Elevation, η_0

FIG. 4. A contour plot of the steady surface elevation η_0. Topography is the model geometry of Fig. 1. The parameters are the same as for Fig. 2; that is, the shelf width is $S = 2a$, the margin width is $M = 0.2$, and the forcing width is $E = 0.05$. The depth ratio is 8. Contoured from 0.4 to 1.3 by 0.1 of the height at the shelf break for large x, σ_3, as defined in the text.

and off the shelf:

$$(R_1^2\nabla^2 - 1)(R_2^2\nabla^2 - 1)(a_1^2\nabla^2 - 1)Z_1 = 0, \quad (28c)$$

where Z is any one of η, ξ', or ξ''. The Rossby radii are $R^2 = g'^{1}h_uh_m/[f^2(h_u + h_m)]$ and $a_s^2 = g(h_u + h_m)/f^2$, where it has been assumed $g'^{1}/g \ll 1$. Off the shelf, assuming both the relation between g and g'^{1} and that $g'^{2}/g'^{1} \ll 1$, the Rossby radii are $a_d^2 = g(h_u + h_m + h_l)/f^2$, $R_1^2 = g'^{1}h_u(h_m + h_l)/(f^2(h_u + h_m + h_l))$, and $R_2^2 = g'^{2}h_mh_l/(f^2(h_m + h_l))$. The assumption that $g'^{2}/g'^{1} \ll 1$ follows from the typical stratification in the coastal area. If g'^{1} represents the main thermocline and g'^{2} crudely represents the deep stratification, it is reasonable to assume $g'^{2} \ll g'^{1}$.

The solution in the absence of a canyon is described in the appendix. The major changes, compared to the homogeneous case, are the presence of two length scales over the shelf (and three off it) and the smoothness of the solutions.

To calculate the solution over the shelf consider the flow in terms of an upper layer streamfunction η, which is simply the surface height and a lower layer streamfunction $\psi = g'/g\eta + \xi'$ where ξ' is the elevation of the interface between the top two layers. From the governing equations and the boundary conditions at the wall and at the shelf break, the perturbation solution (that is, the total solution minus the solution in the absence of the canyon) can be written

$$\eta = \sum_n \sin\left(\frac{n\pi y}{S}\right) [A_n\mathscr{E}_R(x) + B_n\mathscr{E}_a(x)]$$

$$+ \cos\left(\frac{n\pi y}{S}\right) [G_n\mathscr{E}_R(x) + H_n\mathscr{E}_a(x)] \quad (29a)$$

and

$$\psi = \sum_n \sin\left(\frac{n\pi y}{S}\right) [C_n\mathscr{E}_R(x) + D_n\mathscr{E}_a(x)], \quad (29b)$$

where

$$\mathscr{E}_*(x) = \exp\left\{-\frac{x}{*}\left[1 + \left(\frac{n\pi*}{S}\right)^2\right]^{1/2}\right\}, \quad (30)$$

where the asterisk represent the barotropic, a, or the baroclinic, R, Rossby radius and where

$$0 = \sum_n G_n\mathscr{E}_R(x) + H_n\mathscr{E}_a(x) \quad (31)$$

because the streamfunction must be zero at the wall.

The surface will be smooth across the top of the canyon and therefore by symmetry, $\partial\eta/\partial x$ will be zero at $x = 0$ for all y, which implies

$$aA_nP_n = -RB_nQ_n \quad (32a)$$

and

$$aG_nP_n = -RH_nQ_n, \quad (32b)$$
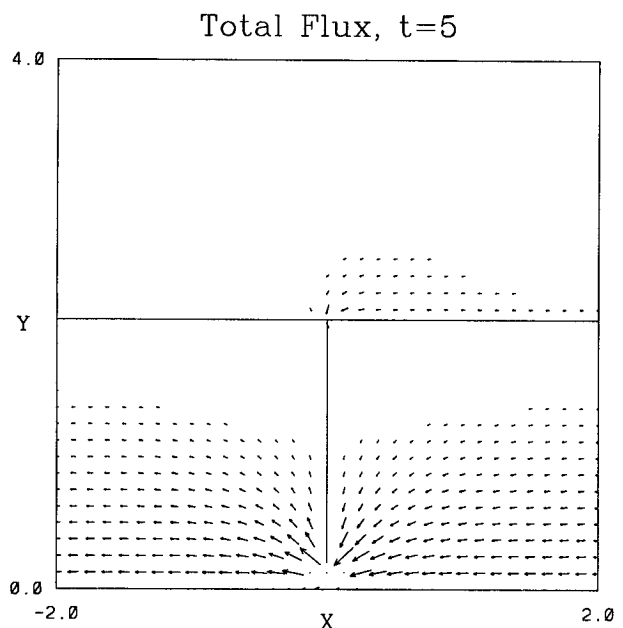
Total Flux, t=5

FIG. 5. The total analytic velocity field after five inertial periods. Parameters same as Fig. 2; the position of the canyon and shelf break are marked.

FIG. 6. Sketch showing the variables for the three-layer model.

where

$$P_n = \left[1 + \left(\frac{n\pi R}{S} \right)^2 \right]^{1/2} \qquad (33a)$$

and

$$Q_n = \left[1 + \left(\frac{n\pi a}{S} \right)^2 \right]^{1/2}. \qquad (33b)$$

The combination of (31) and (32b) imply G_n and H_n are zero.

As well as the boundary condition that ψ is a uniform over the canyon and equal to the value over the shelf break (because there is no growing middle layer flow over either), we need two further constraints to determine A_n, B_n, C_n, and D_n. A mass balance in each of the two layers provides these constraints. The increasing thickness perturbation of each layer must be balanced by the constant perturbation flux into that layer. Consider a rectangle against the coast, $0 \leqslant y \leqslant Y$ and $0 < x < \infty$. For the upper layer the above balance implies

$$\int_0^\infty dx \int_0^Y dy (\eta - \xi) = - \int_0^\infty dx (v_0 h_u)|_{y=Y}$$

$$- \int_0^Y dy (u_0 h u)|_{x=0}, \qquad (34)$$

as the perturbation is expected to be localized to the canyon region and there can be no flux through the wall. The flux due to the Ekman pumping is accommodated by the flow in the absence of the canyon (we are considering the perturbation to that flow not the total flow). Expanding, integrating, and substituting expressions for η and ξ gives

$$\sum_n \sin\left(\frac{n\pi y}{S} \right) \left[A_n \left(\frac{R}{P_n} - \frac{l^2}{RP_n} \right) \right.$$

$$\left. + B_n \left(\frac{a}{Q_n} - \frac{l^2}{aQ_n} \right) - E_n \frac{R}{P_n} - F_n \frac{a}{Q_n} \right] = 0, \quad (35)$$

where

$$\xi = \sum_n \sin\left(\frac{n\pi y}{S} \right) [E_n \mathcal{E}_R(x) + F_n \mathcal{E}_a(x)], \quad (36)$$

and $l^2 = gh_u/f^2$. As (35) must be valid for all y, it must be valid for each n separately. Analogous manipulation for the middle layer gives

$$C_n L^2 a Q_n + D_n L^2 RP_n - E_n R^2 a Q_n - F_n a^2 RP_n = 0, \quad (37)$$

where $L^2 = g'^{-1}h_m/f^2$.

The three conditions, (32a), (35), and (37), and the definition of ψ, which links C_n with A_n and E_n and which links D_n with B_n and F_n, allow the calculation of C_n in terms of D_n. In terms of $I_n = C_n + D_n$ the boundary conditions on the middle layer at $x = 0$ are

$$\psi_S - \psi_0 = \sum_n \sin\left(\frac{n\pi y}{S} \right) I_n, \quad y > M \quad (38a)$$

and

$$0 = \sum_n \sin\left(\frac{n\pi y}{S} \right) \frac{P_n}{R} I_n, \quad y < M, \quad (38b)$$

assuming $g'^{-1}/g \ll 1$. The solution method follows the homogeneous case using a Fourier sum. The
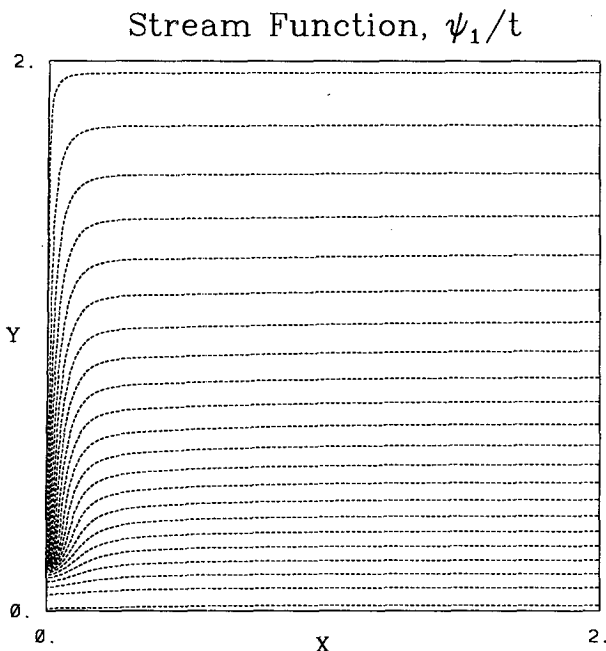
Stream Function, ψ_1/t

FIG. 7. Middle-layer streamfunction for the three-layer model with topography of Fig. 1. The shelf width is $S = 2a_s$, the margin width is $M = 0.2a_s$, and the forcing width is $E = 0.05a_s$. The stratification is $g'^1 = 0.1$ m s^{-2}, $h_u = 30$ m, maximum $h_m = 70$ m, and $h_l = 300$ m.

streamfunction for the middle layer is illustrated in Fig. 7.

For a barotropic fluid the total flux is $2a_s^2 q_0 \sinh(E/a_s)$ for the canyon of Fig. 1, whereas for a stratified fluid (with stratification given above) it is $8a_s^2 q_0 \sinh(E/a_s)$. The large enhancement is due to the smaller length scale, the baroclinic Rossby radius, which increases the flux for a given change in streamfunction. Physically, consider the excess mass required over the canyon in order for the flow to be deflected around the canyon. For a long canyon, the mass accumulated over the canyon is given by the (canyon length) × (the appropriate Rossby radius) × (the appropriate height scale). So the ratio of the baroclinic to the barotropic case is

$$\frac{(S - M)(R)(g/g'q_0 \sinh E)}{(S - M)(a)(q_0 \sinh E)}, \quad (39)$$

which gives an enhancement of 5 times for this case, very close to the 4 times found from the full calculation.

The lower-layer velocity must be parallel to the shelf break and canyon walls, which implies the pressure in the lowest layer must be uniform along them. The growing pressure (ψ) is uniform along the topography in the middle layer; thus, the growing interface elevation between the lowest and middle layers must also be uniform along the shelf break and through the canyon. The canyon brings this higher interface height into the shelf region and allows it to exist over a larger area,

the whole area of the canyon. The deep-water flux into the canyon is simply the length of the canyon multiplied by the elevation of the interface at the shelf break. In a nonlinear flow a sink for middle layer fluid will cause the interface between the lower layer and the middle layer to rise and will, therefore, further enhance the flux of deep water into the canyon. This effect is the problem of selective withdrawal in a rotating fluid; it has been considered by Monismith and Maxworthy (1989) and McDonald and Imberger (1992).

4. Steady solution

As time progresses, assuming a constant wind stress, the flow over the shelf will reach a finite velocity controlled by the forcing, by lateral viscosity and by bottom friction. Lateral viscosity is only important over distances of order $([2A_hh]/[\delta f])^{1/2} \approx 14$ km, where $\delta = (2A_v/f)^{1/2}$ is the Ekman layer thickness and A_h and A_v are the horizontal and vertical eddy viscosities. The inclusion/exclusion of lateral viscosity does not change the basic dynamics, so, for clarity, we will neglect lateral viscosity. Bottom friction will generate a bottom Ekman layer, including its effects on the flow; the linear barotropic shallow water equation, (1a) remains the same but (1b) becomes

$$\frac{\partial \eta}{\partial t} + \nabla \cdot (h\mathbf{u}) = \frac{1}{2} \delta \nabla \times \mathbf{u}. \quad (40)$$

The boundary layer at the coast where the bottom Ekman layer rises into the fluid and the upper Ekman layer is formed is not modeled. The modified potential vorticity equation is

$$\frac{\partial}{\partial t}\left(\eta - \frac{\lambda h}{f}\right) = \mathbf{u} \cdot \nabla h + \lambda \frac{\delta}{2}, \quad (41)$$

where $\lambda = \nabla \times \mathbf{u}$ and we have assumed the wind stress is uniform. In the steady state, $\partial/\partial t = 0$ so the right-hand side must also be zero. If we consider the shelf itself (where ∇h is assumed zero) we have $\lambda = 0$. In the steady state, one can show that $\lambda = g/f\nabla^2\eta$. Thus, the governing equation is a Laplace equation,

$$\nabla^2\eta = 0. \quad (42)$$

The potential vorticity conservation (41) implies that there is no geostrophic flow over the shelf break or canyon walls to order δ/h. Thus, the surface height η must be uniform over these depth changes. In summary, we have a Laplacian rather than a modified Helmholtz equation and we have the same boundary conditions. The solution in the absence of the canyon is given in the appendix.

The Laplace equation leads to a solution similar to the Helmholtz equation solution but the scale is determined by the shelf width rather than the Rossby radius. The solution for η can be found analytically through a conformal mapping (Naasse and Kabbaj 1990) but, for

TABLE 1. A list of the parameters used in the numerical model.

| | Run | | | | | | | |
	1	2	3	4	5	6	Astoria	Tully
Stratified	No	Yes	No	Yes	Yes	Yes	Yes	No
Nonlinear	No	No	Yes	Yes	Yes	Yes	Yes	Yes
Bottom friction	No	No	No	No	No	No	No	Yes
Topography	Model	Model	Model	Model	Model	Model	Astoria	Tully
E (km)	11.1	11.1	11.1	11.1	11.1	11.1	38.1	4.0
q_0 (m s^{-1})	1.6e$-$10	1.6e$-$10	1.6e$-$10	1.6e$-$10	1.6e$-$5	1.3e$-$4	4.0e$-$05	9.4e$-$04
τ (m^2 s^{-2})	1.7e$-$10	1.7e$-$10	1.7e$-$10	1.7e$-$10	1.7e$-$5	1.4e$-$4	1.5e$-$04	3.7e$-$04
Forcing								
ramped up ($2\pi/f$)	1	1	1	1	1	0.5	No	No
steady ($2\pi/f$)	∞	∞	∞	∞	3	0	∞	∞
ramped down ($2\pi/f$)	No	No	No	No	1	0.5	No	No
depth (m)								
Upper-layer	na	30	na	30	30	30	40	na
Middle-layer	na	70	na	70	70	70	160	na
Lower-layer	na	300	na	300	300	300	700	na
δ (m)	na	na	na	na	na	na	na	15

consistency, was found using the Fourier transform technique used for the Helmholtz equation in section 2. The surface height is expanded as

$$\eta = \sum_{n=1}^{\infty} c_n \sin\left(\frac{n\pi y}{S}\right) \exp\left(\frac{-n\pi x}{S}\right), \quad (43)$$

and the c_n are determined by the boundary conditions through a truncated sum and inverting the resulting matrix. The flux through the canyon is given by

$$2qE \sum_n c_n \left[(-1)^n - \cos\left(\frac{n\pi M}{S}\right) \right], \quad (44)$$

which is, for the canyon of Fig. 1, $6qEa$. Note that the flux is independent of δ, the Ekman layer thickness, and therefore is independent of the value of the eddy viscosity. However, the theory is based on the assumption of a constant eddy viscosity. Note also that this solution is a solution of the full nonlinear equations, but it is not unique.

5. Results from a linear numerical model

a. Homogeneous case—run 1

A homogeneous primitive shallow-water equation model was run to model the canyon of Fig. 1, that is,

TABLE 2. Parameters of the various topographies used in the numerical model.

Topography	Model	Astoria	Tully
Shelf depth (m)	50	135	100
Off-shelf depth (m)	400	900	250
Canyon bottom	flat	sloping	flat
Canyon width (km)	22.2	6.4	8.0
Margin (km)	44.3	17.0	47.0
Canyon length (km)	404.7	21.1	43.0

a canyon cutting into a shelf 50 m deep from 400 m [but the width of the canyon (22 km) is necessarily finite]. The model is a finite-difference, leapfrog solution of the layered shallow-water equations (1) and is described in Allen (1988). The forcing consists of removal of fluid at the closest grid point to the wall. In order to be consistent with linear dynamics this rate is very small, 0.014 mm/day, and is equivalent to a wind stress of 1.7×10^{-10} m^2 s^{-2}. A list of parameters is
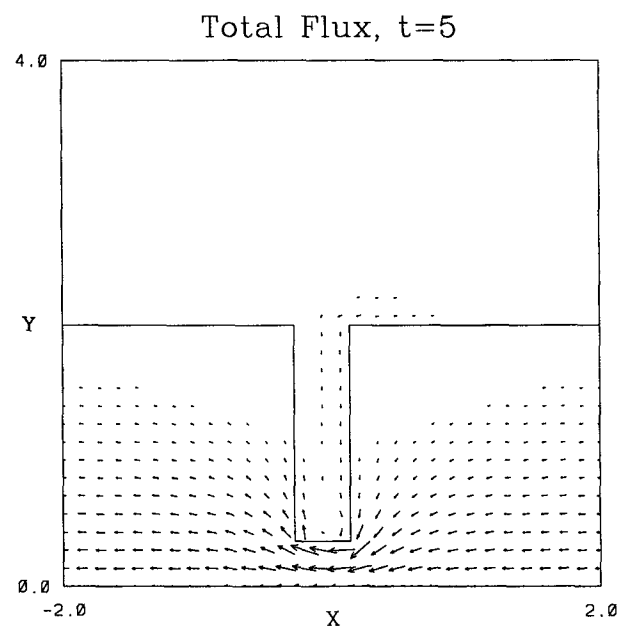

FIG. 8. Results from the linear, homogeneous numerical model (run 1). The total flux at five inertial periods. Parameters are listed in Table 1. The topography is the model topography described in Table 2.

Run 2—— Upper Layer Velocity

Run 2——Upper Layer Vorticity

Run 2—— Middle Layer Velocity
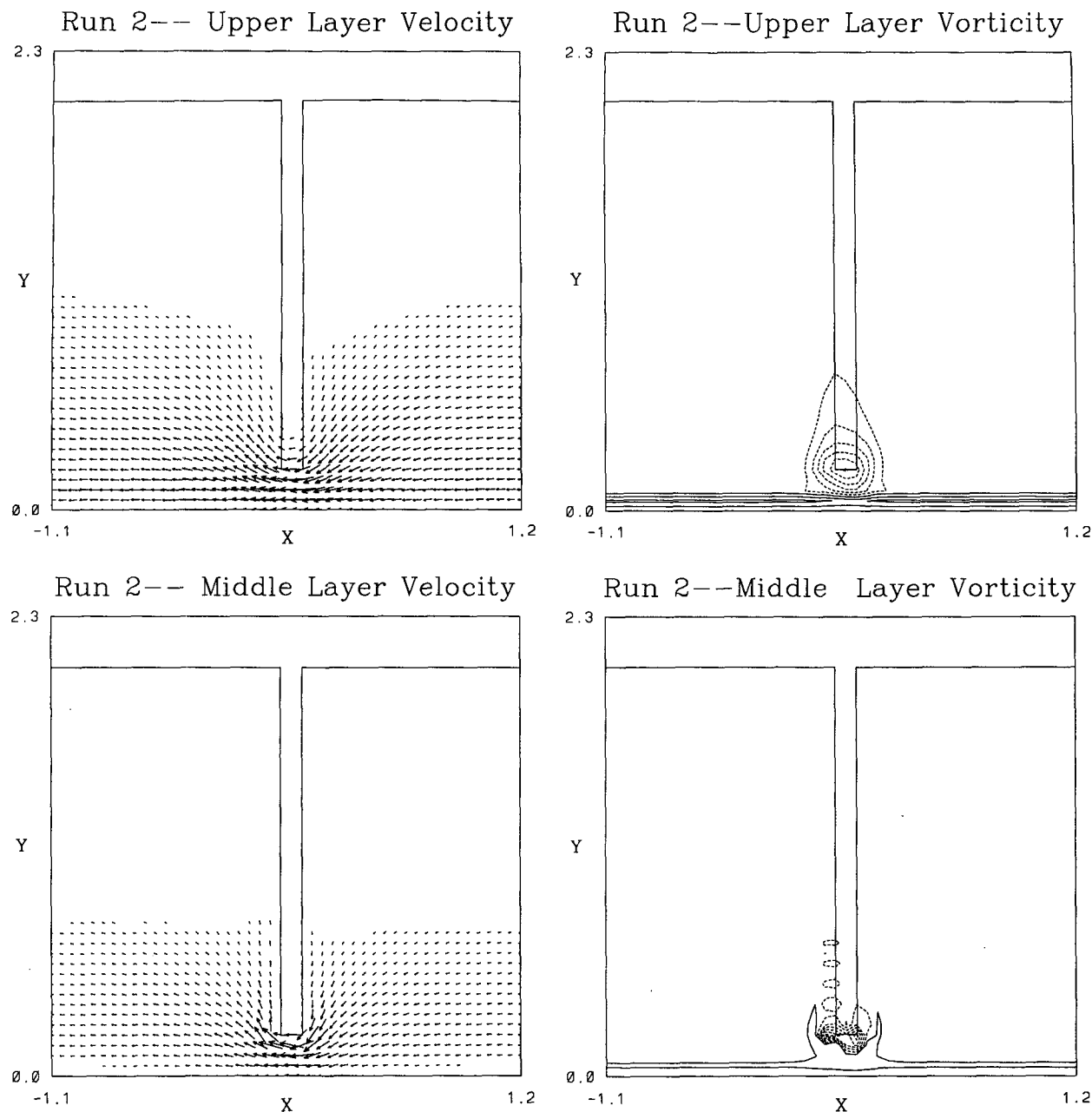
Run 2——Middle Layer Vorticity

FIG. 9. Results from the linear, stratified numerical model (run 2) 100 hours after forcing started. (a) The upper-layer velocity, maximum velocity vector is 1.8 mm s^{-1}. (b) The upper-layer vorticity, contoured from $-1.3 \times 10^{-6}f$ to $6.8 \times 10^{-7}f$ by $2.2 \times 10^{-7}f$. (c) The middle-layer velocity, maximum velocity vector is 2.2 mm s^{-1}. (d) The middle-layer vorticity, contoured from $-5.2 \times 10^{-6}f$ to $3.4 \times 10^{-7}f$ by $1.1 \times 10^{-6}f$.

given in Table 1 for the various numerical runs (this is run 1) and for the various topographies in Table 2. The grid spacing is equal to the distance between the arrows in each of the plots. The grid spacing was increased to confirm that the flow was well resolved.

To compare with the analytic model, the total flux is plotted in Fig. 8 at the fifth pendulum day. The velocities at the head of the canyon are slightly smaller than

for an infinitesimally thin canyon. The flux propagating along the shelf break and through the canyon is clearly evident and dominates the flux (but not the velocity) over the outer shelf. The flow pattern on either side of the canyon is clearly similar to the flux plot shown in Fig. 3.

The topographic waves, which establish the flow pattern seen in Fig. 8, propagate fast enough that the

Run 2—— Lower Layer Velocity

Run 2——Lower Layer Vorticity

Run2——Interface Height ξ^I

Run2——Interface Height ξ^{II}
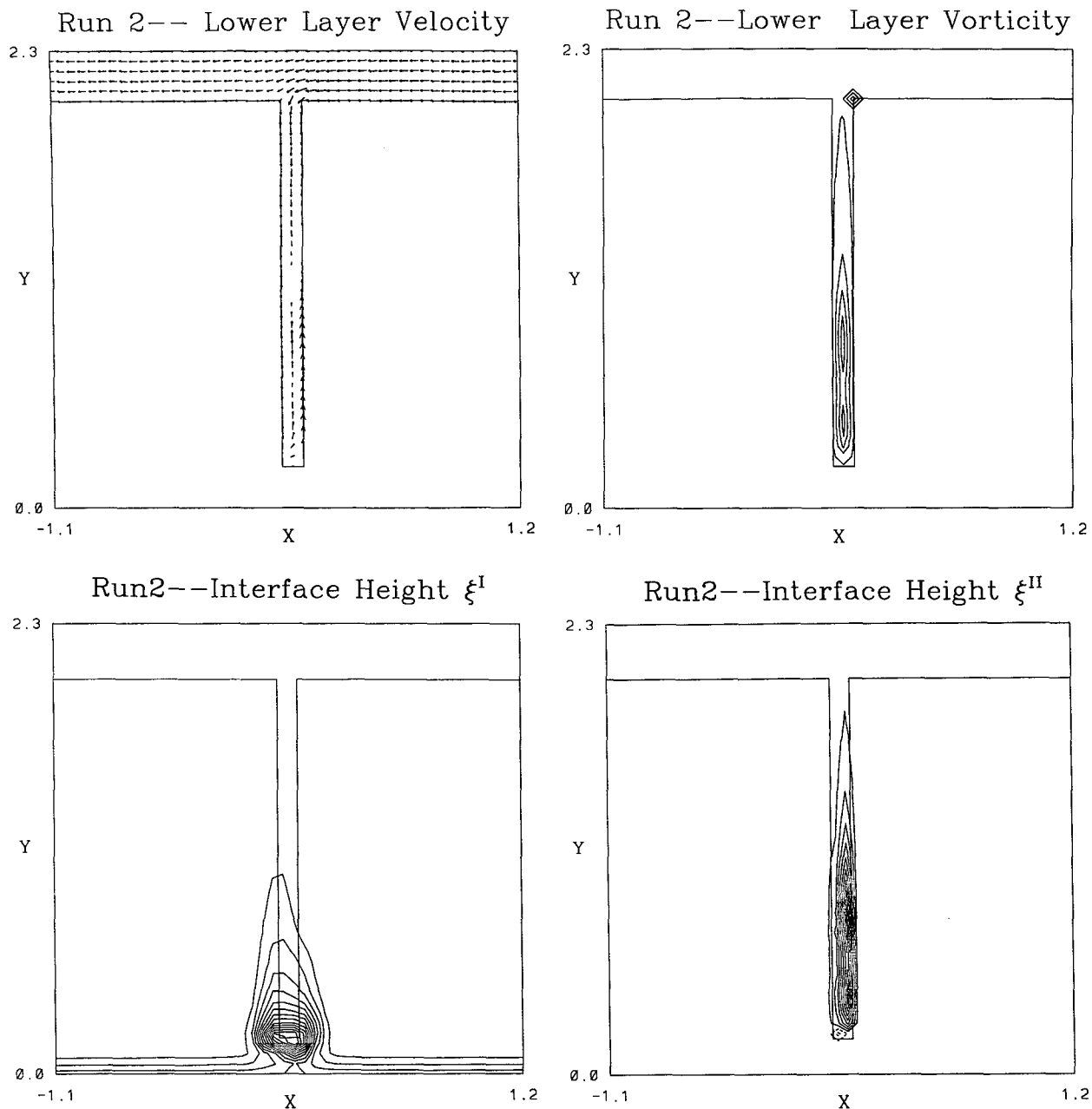
FIG. 9. (*Continued*) (e) The lower-layer velocity, maximum velocity vector is 0.27 mm s^{-1}. (f) The lower-layer vorticity, contoured from $2.2 \times 10^{-9} f$ to $9.2 \times 10^{-8} f$ by $2.2 \times 10^{-8} f$. (g) The interface between middle and upper layer, contoured from 3×10^{-3} mm to 4.2×10^{-2} mm by 3×10^{-3} mm. (h) The interface between lower and middle layer, contoured from -1.3×10^{-2} mm to 4.2×10^{-2} mm by 5×10^{-3} mm.

flow is very close to equilibrium after two inertial periods. Note that the double Kelvin waves do not "start" until Poincaré waves have propagated the information of the sink at the coast to the shelf break. The flow adjusts even more quickly for the more realistic canyons considered in sections 6c and 6e as they are shorter.

The canyon in the numerical model (and in the field) is not infinitesimally thin but is very thin compared to the barotropic Rossby radius. The two solutions (the numerical and the analytic) do not differ significantly. The surface over the finite width canyon (as shown by the numerical model) is almost flat across the canyon. However, the velocities in the deep ocean are smaller

Run 5— Upper Layer Velocity

Run 5—Upper Layer Vorticity

Run 5— Middle Layer Velocity

Run 5—Middle Layer Vorticity
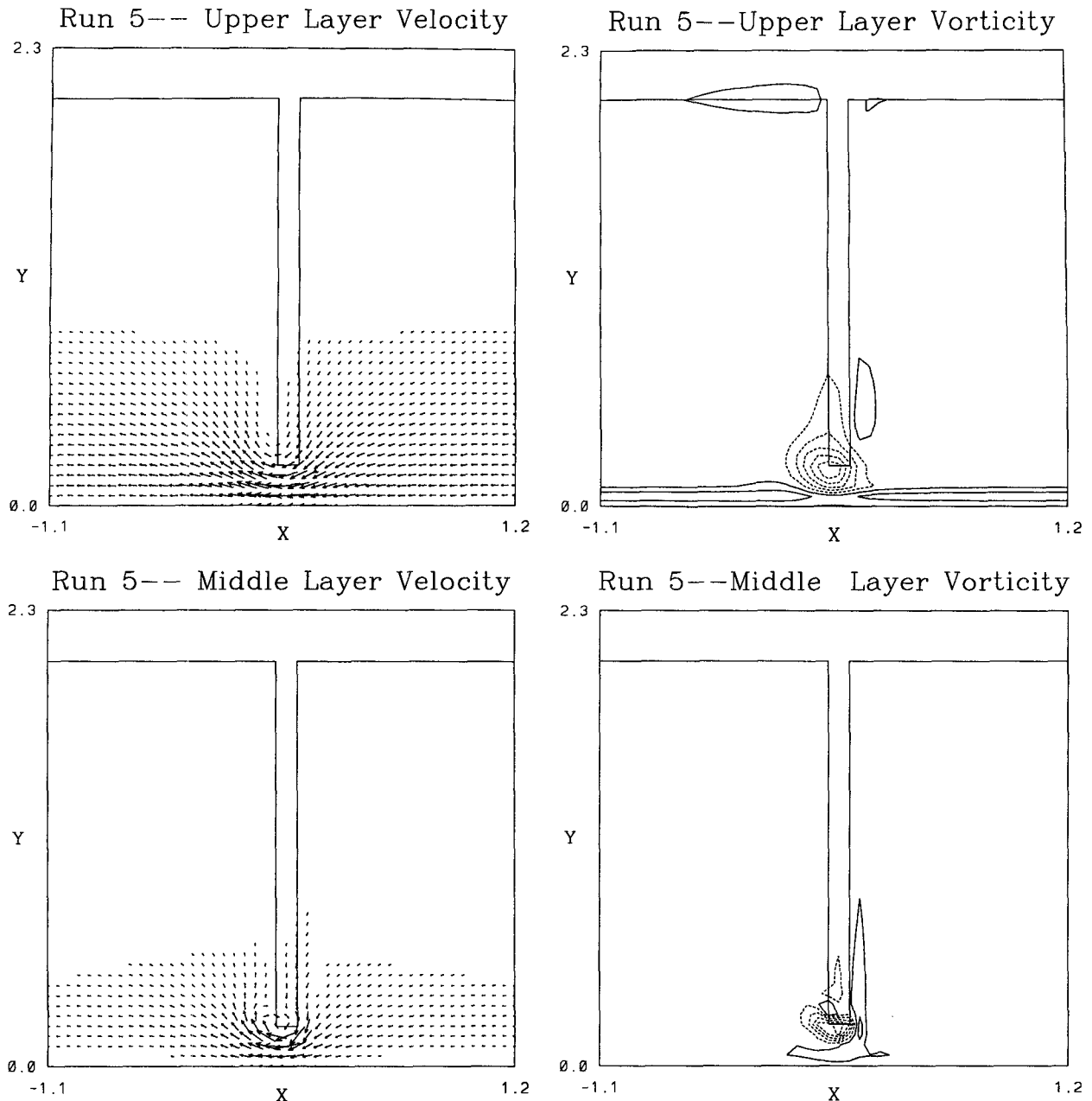
FIG. 10. Results after 103 hours for the nonlinear, stratified numerical model (run 5) with forcing spread over 87 hours. (a) The upper-layer velocity, maximum velocity vector is 53 cm s^{-1}. (b) The upper-layer vorticity, contoured from $-0.11f$ to $0.023f$ by $0.022f$. (c) The middle-layer velocity, maximum velocity, vector is 70 cm s^{-1}. (d) The middle-layer vorticity, contoured from $-0.53f$ to $0.15f$ by $0.11f$.

than for the analytic solution due to the width of the canyon.

b. Stratified case—run 2

The model was run with three layers, using the same parameters as the case described in section 3 and Fig. 6. The lowest layer intersects the topography along the canyon and shelfbreak walls. The code can handle the intersection with topography provided the intersection line does not move more than half a grid cell size. The lower layer is assumed to slip freely along the topography. The layered model has advantages in that it replicates the stratification used in the analytic model and can handle steep topography (up to the point where the hydrostatic approximation is no longer valid).

The velocity, vorticity, and interface heights are shown in Fig. 9. The equilibrium solution described in
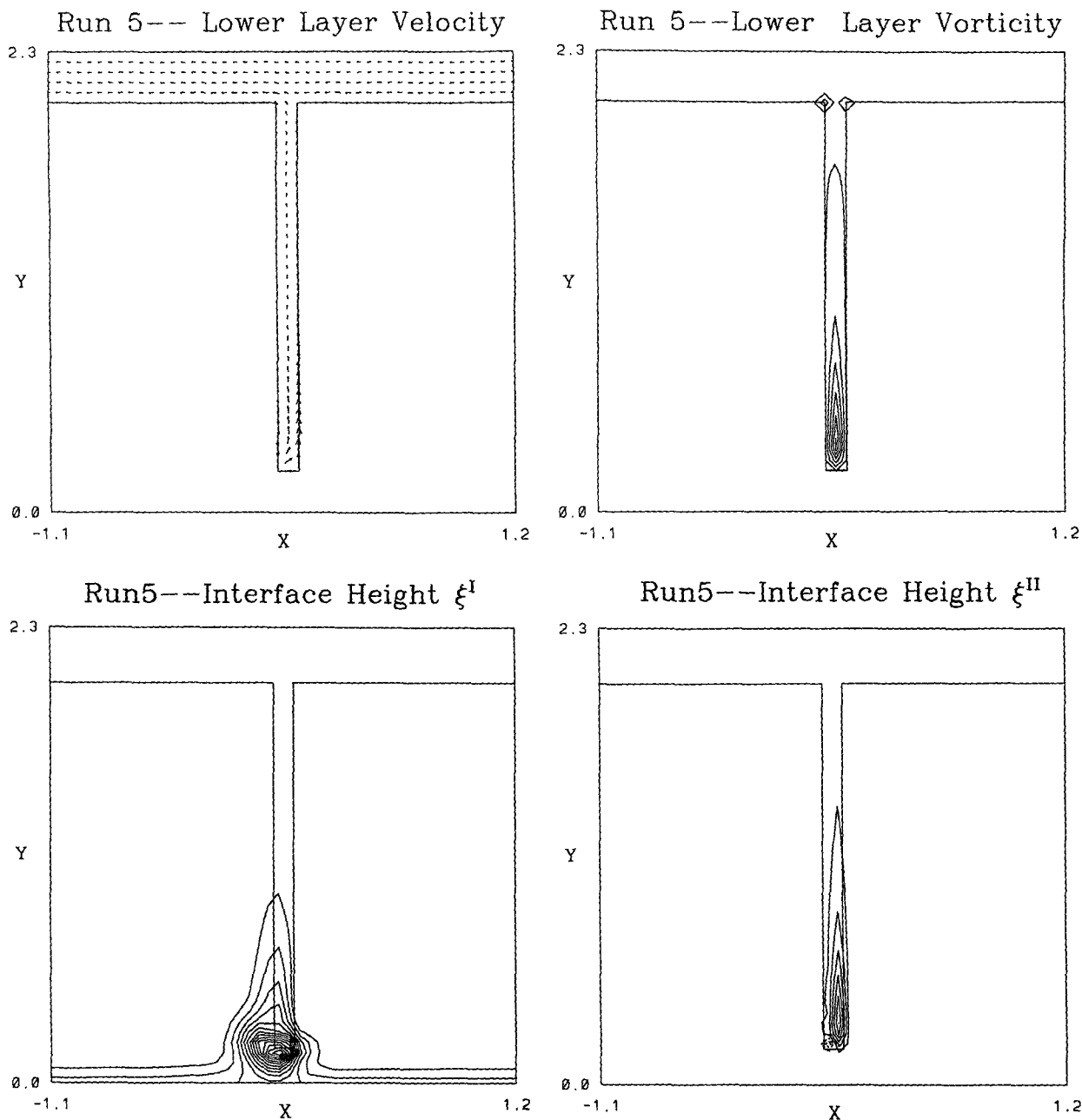
Run 5— Lower Layer Velocity

Run 5——Lower Layer Vorticity

Run5——Interface Height ξ^{I}

Run5——Interface Height ξ^{II}

FIG. 10. (*Continued*) (e) The lower-layer velocity, maximum velocity vector is 14 cm s^{-1}. (f) The lower-layer vorticity, contoured from $-2.2 \times 10^{-4}f$ to $3.4 \times 10^{-2}f$ by $5.6 \times 10^{-3}f$. (g) The interface between middle and upper layer, contoured from 30 cm to 4.5 m by 30 cm. (h) The interface between lower and middle layer, contoured from -5 m to 16 m by 3 m.

section 3 is closely approached by the third inertial period except in the lower layer. The start of the forcing causes very strong upwelling in the head of the canyon, given approximately by $2\eta_1 fg/g''$, and grows with a half-life of about two inertial periods. This accumulated volume of deep water slowly dissipates thereafter, traveling along the upstream side of the canyon (Fig. 9h). It is a slow process, consistent with a second baroclinic

mode Kelvin wave type phenomenon. The wave front is less than halfway down the canyon after ten inertial periods (Fig. 9e). The fluid traveling up the canyon increases the lower-layer depth generating cyclonic vorticity (Fig. 9f) by conservation of potential vorticity. This vorticity scales as $f\eta_2/h_1$.

The upper-layer flow is strongly bent over the canyon (Fig. 9a) by the vorticity (Fig. 9b) due to the up-

Run 6—— Upper Layer Velocity

Run 6——Upper Layer Vorticity

Run 6—— Middle Layer Velocity
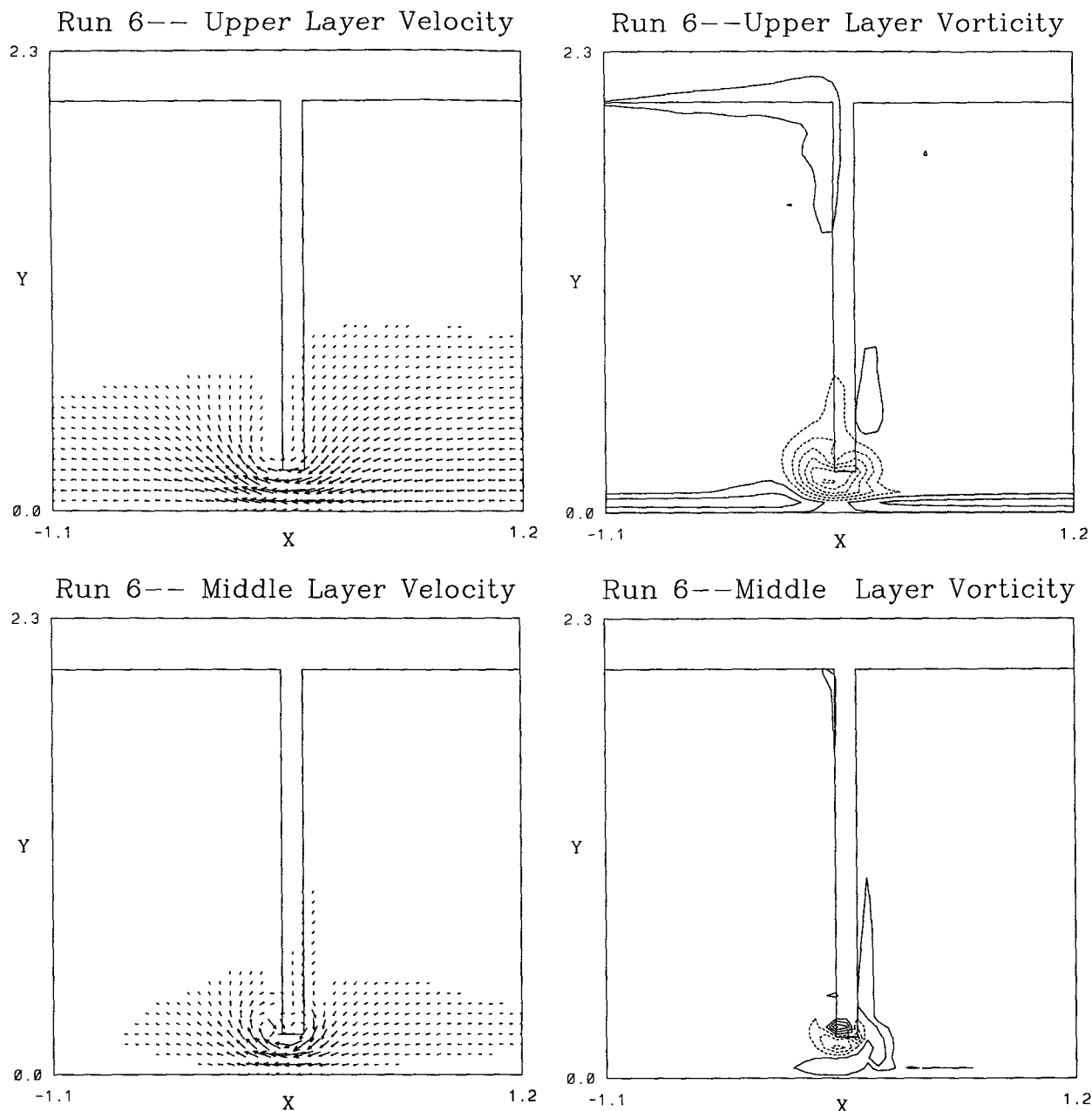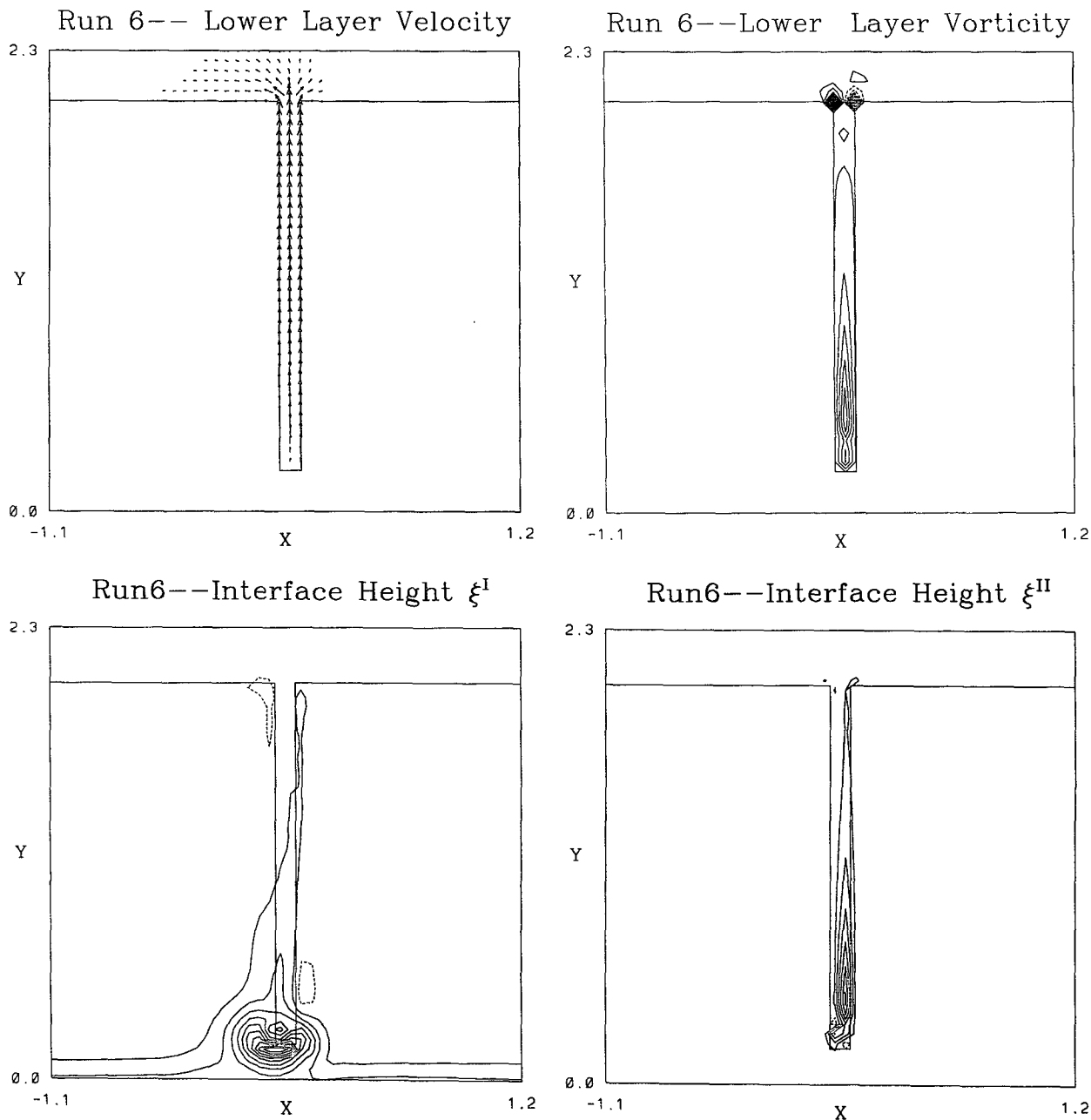
Run 6——Middle Layer Vorticity

FIG. 11. Results after 103 hours for the nonlinear, stratified numerical model (run 6) with forcing spread over 17 hours. (a) The upper-layer velocity, maximum velocity vector is 57 cm s^{-1}. (b) The upper-layer vorticity, contoured from $-0.13f$ to $0.025f$ by $0.022f$. (c) The middle-layer velocity, maximum velocity vector is 76 cm s^{-1}. (d) The middle-layer vorticity, contoured from $-0.64f$ to $0.70f$ by $0.22f$.

ward movement of the interface height (Fig. 9g), which reduces the upper-layer depth. By conservation of potential vorticity this leads to anticyclonic vorticity as is seen. The middle-layer growing velocity (all that is visible in Fig. 9c) cannot cross the canyon and is bent sharply around the end. The necessary vorticity (Fig. 9d) is generated by fluid upwelling onto the shelf from the canyon. This fluid also increases the interface

height (Fig. 9g), which changes the vorticity in the upper layer.

6. Results from a nonlinear numerical model

a. Test cases—runs 3 and 4

The nonlinear numerical model used the discretization of Arakawa and Lamb (1981), which does not

Run 6—— Lower Layer Velocity

Run 6——Lower Layer Vorticity

Run6——Interface Height ξ^{I}

Run6——Interface Height ξ^{II}

FIG. 11. (*Continued*) (e) The lower-layer velocity, maximum velocity vector is 28 cm s^{-1}. (f) The lower-layer vorticity, contoured from $-8.9 \times 10^{-2}f$ to $0.1f$ by $5.6 \times 10^{-3}f$. (g) The interface between middle and upper layer, contoured from -30 cm to 4.7 m by 50 cm. (h) The interface between lower and middle layer, contoured from -2 m to 16 m by 3 m.

have the nonlinear instability problems of the discretization used for the nonlinear code of Allen (1988). Two cases, one stratified and one homogeneous, were run with very small forcing in order to compare with the linear code. The Arakawa and Lamb scheme has a larger "footprint," which leads to smoothing, but otherwise the results were very similar. The velocity fields are almost indistinguishable but the vorticity pat-

tern has a slightly larger spatial extent for the nonlinear run (not shown).

b. Effect of advection and the forcing timescale— runs 5 and 6

The model canyon was run for two cases, one with very strong forcing (equivalent to a wind stress maxi-

Astoria Upper Layer Velocity

Astoria Upper Layer Vorticity

Astoria Middle Layer Velocity

Astoria Middle Layer Vorticity
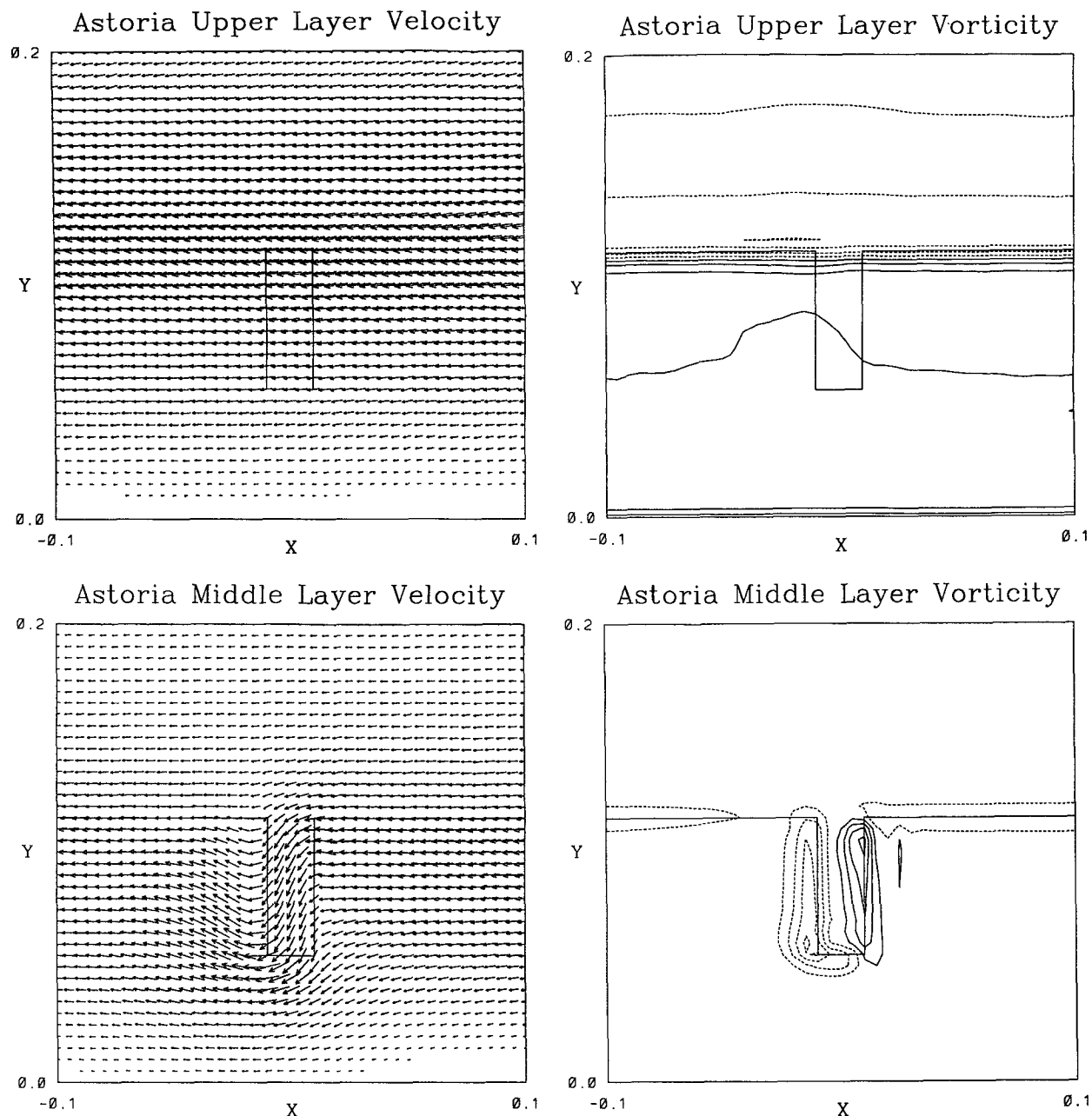
FIG. 12. Results after 24 hours for the nonlinear, stratified numerical model (run Astoria) over Astoria topography (see Table 2). (a) The upper-layer velocity, maximum velocity vector is 22 cm s^{-1}. (b) The upper-layer vorticity, contoured from $-0.11f$ to $0.062f$ by $0.025f$. (c) The middle-layer velocity, maximum velocity vector is 13 cm s^{-1}. (d) The middle-layer vorticity, contoured from $-0.43f$ to $0.43f$ by $0.12f$.

mum of 1.4×10^{-4} m^2 s^{-2}) over a short time (one inertial period) and the other with the same total forcing spread over a longer time [maximum wind stress $(1.7 \times 10^{-5}$ m^2 s$^{-2})$ spread over 5 inertial periods]. Thus, run 6 is a short sharp wind event and run 5 is a less severe but longer wind event.

First, compare run 5 with the linear run 2. The main effect of the nonlinear terms is to sweep the pattern

(flow toward the coast followed by flow seaward) farther downstream. In Fig. 9a, the upper-layer flow pattern is centered over the canyon; in Fig. 10a it is over the downstream edge of the canyon. This effect is much stronger for a realistic shelf current/canyon (such as Astoria, see later) than it is for the extreme model canyon. The second effect of the nonlinear terms is to advect the potential vorticity distribution, which in turn
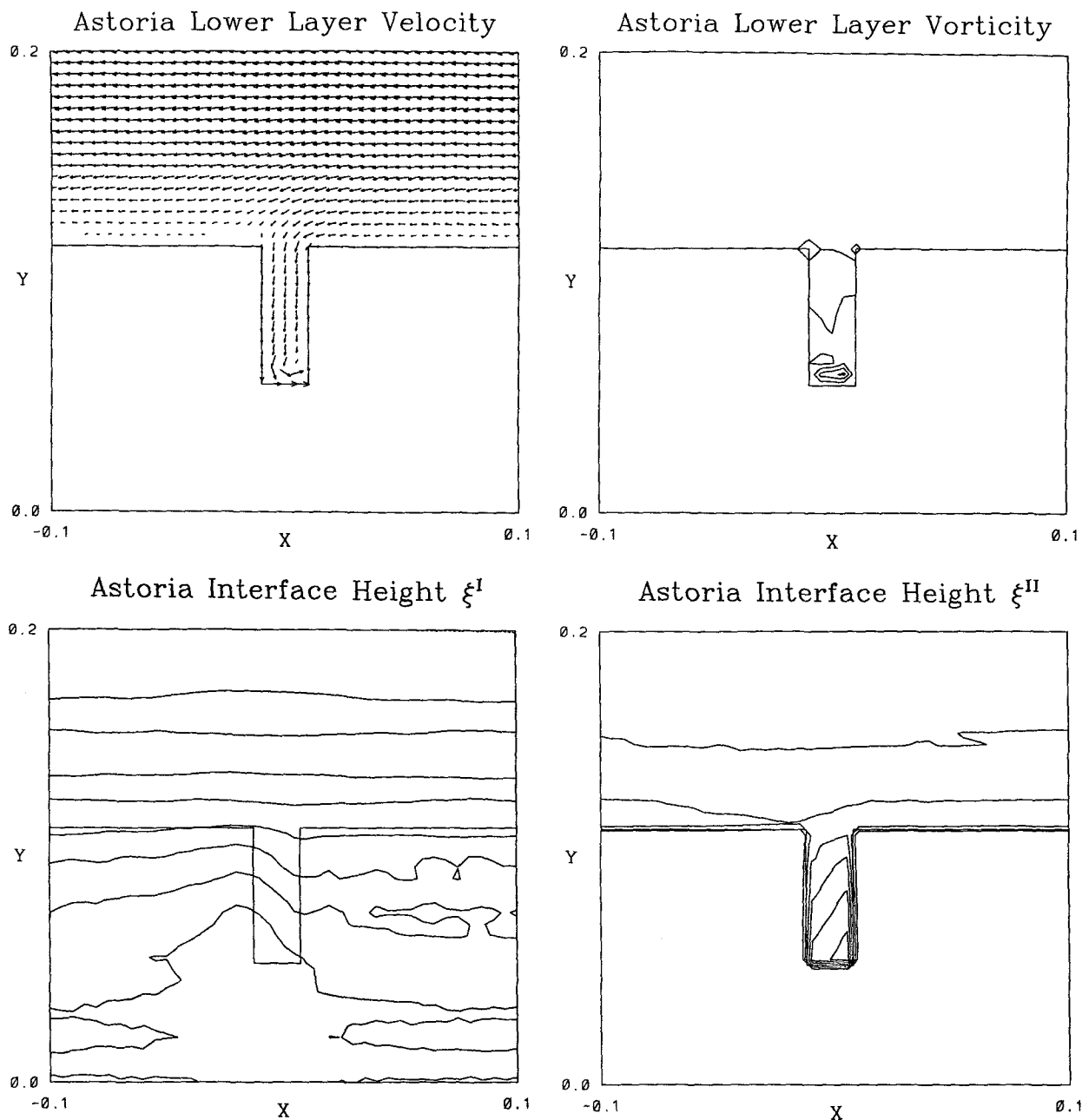
Astoria Lower Layer Velocity

Astoria Lower Layer Vorticity

Astoria Interface Height ξ^I

Astoria Interface Height ξ^{II}

FIG. 12. (*Continued*) (e) The lower-layer velocity, maximum velocity vector is 2 cm s^{-1}. (f) The lower-layer vorticity, contoured from $0f$ to $0.19f$ by $0.062f$. (g) The interface between middle and upper layer, contoured from -30 cm to 4.2 m by 50 cm. (h) The interface between lower and middle layer, contoured from 3 m to 18 m by 3 m.

modifies the flow pattern. For the linear run the flow pattern in the middle layer is a simple U shape around the end of the canyon (Fig. 9c). However, in the non-linear case the advection of the fluid originally in the canyon has caused a strong anticyclonic circulation with closed streamlines (Fig. 10c).

The movement of the potential vorticity depends not only on the total strength of the flow but also on the history of the flow. Flow that is strong in the early stages, before the topographic waves have a chance to establish the equilibrium solution, causes more modification of the potential vorticity distribution because at this stage the flow is across the topography and thus across the strong potential vorticity gradients. Compare run 5 (Fig. 10c) to run 6 (Fig. 11c). In run 6 there are multiple eddies in the middle layer and almost a closed

TABLE 3. Variations of parameters used in the numerical model of Astoria Canyon. The first column gives a run number, the second the change in the parameter, the third the appropriate nondimensional number and its change, and the last six columns show the presence of the change in the field. An "s" indicates the change was minor and not dependent on the given nondimensional number.

Run	Parameter	Nondimensional number	η	u_1	ξ^I	u_2	ξ^{II}	u_3
A1	$g'' \times 5$	$\bar{u}_2/fg'^2 \times 0.5$				x	x	x
A2	$g'^2 \times 5$	$\bar{u}_2/fg'^2 \times 5$					x	x
A3	$h_1 \times 1/2,\ h_2 \times 9/8$	$\Delta h_2/h_2 \times 0.6$				x		x
A4	$h_2 \times 5/4,\ h_3 \times 0.91$	$\Delta h_2/h_2 \times 1.4$				x	x	x
A5	flat canyon	$(g'^2 h_3)^{1/2}f/L \times 1.2$	s		s			x
A6	forcing at wall	$\bar{u}_2/fg'^2 \times 0.94$					x	x
A7	forcing $\times 2.0$	$\bar{u}_2/fg'^2 \times 2.0$		x	x		x	x

eddy in the upper layer. Cyclonic vorticity (Fig. 11d) occurs over the downstream edge of the canyon where the original anticyclonic eddy has caused shelf fluid to fall into the canyon. The relaxation of the forcing has allowed the lower layer to adjust more quickly (hence the flood leaving the canyon in Fig. 11f).

Thus, a true measure of the nonlinearity depends on the competition of the topographic waves and the advection. The topographic wave speed for waves in the canyon is approximately $(g\Delta h)^{1/2}$, where Δh is the difference in depth between the canyon and the shelf (Gill et al. 1986; see also Chen and Allen 1996 for the complete solution). The time for these waves to propagate around the canyon is $2L/(g\Delta h)^{1/2}$ where L is the length of the canyon. If in this time the flow has been strong enough to advect fluid across the canyon, the flow is nonlinear.

For the model canyon, the timescale is slightly over one inertial period. Over this time the slowly forced run 5 has reached only one-eighth of its final velocity and the advection is only one-tenth of the width of the canyon. For the quickly forced run, the advection is a full half of the canyon width.

c. Astoria Canyon

The nonlinear simulation was run for a representation of Astoria Canyon. The model canyon has a sloping bottom cutting into a shelf 135 m deep from 900 m. Three layers were used. The top layer is 40 m deep, the middle layer has maximum thickness of 160 m, and lowest layer has a maximum thickness of 700 m. The canyon bottom slopes slowly (over 19 km) from 900 m to 270 m and then quickly (over 1.6 km) to merge with the shelf. The steep section at the end accommodates the break between the lowest and the middle layer. The stratification between the upper and middle layer is strong ($g'^1 = 0.1$) to represent the thermocline, whereas the stratification between the middle and lower layer is much weaker ($g'^2 = 0.01$) to represent the deep stratification crudely.

In order to force a shelfbreak current as opposed to a current closer to the coast, E, the forcing region, was set equal to S, the shelf width. In the absence of a

canyon, a strong current forms over the shelf break and decays exponentially in both directions. Water was removed from the shelf region at a constant rate of 2.5 meters per inertial period, equivalent to a wind stress of 1.5×10^{-4} m^2 s^{-2}; this value was chosen to give the 25 cm s^{-1} upper-layer velocities observed in the field. The bottom frictional effects were not included as the model was run for only one day to simulate the acceleration phase of the flow.

The major effect of the nonlinear terms is to sweep the inflow/outflow pattern downstream as shown in Fig. 12c. Thus, the inflow branch actually lies over the canyon, leading to very large flows over the canyon, and the outflow branch lies much farther downstream. This latter branch has been observed south of Astoria Canyon (B. Hickey 1993, personal communication).

Figure 12d shows the vorticity in the middle layer. Strong cyclonic vorticity is observed in the middle layer over the upstream side of the canyon. This vorticity is caused by fluid columns being strongly stretched as they "fall" over the lip of the canyon. Flow in the lowest layer is primarily cyclonic with the strongest vorticity at the head (Fig. 12f). Both these effects have been observed over Astoria Canyon (B. Hickey, submitted to J. Phys. Oceanogr. 1996).

There is a local ridge of depression in the interface between the upper two layers at the upstream side of the canyon and a stronger ridge of elevation over the downstream side of the canyon (Fig. 12g). A sigma-t pattern of this form was observed at about $\sigma_t = 26.68$ over the head of Astoria Canyon on 14 August 1978 (Hickey 1987: Fig. 2.48).

The lowest layer is thickest on the upstream side of the canyon (Fig. 12h). The opposite was observed on 14 August 1978 (Hickey 1987: Fig. 2.48) at $\sigma_t = 26.705$ or 26.74. The difference could, perhaps, be due to timing. At earlier times (12 h after forcing begins) the model shows a lower layer deepest at the downstream side of the canyon, near the head.

d. Astoria Canyon—parameter variation

Section 6b considered the effect of the time history of the forcing. In this section, using the Astoria Canyon

Astoria Middle Layer Velocity

Astoria Middle Layer Vorticity

Astoria Middle Layer Velocity
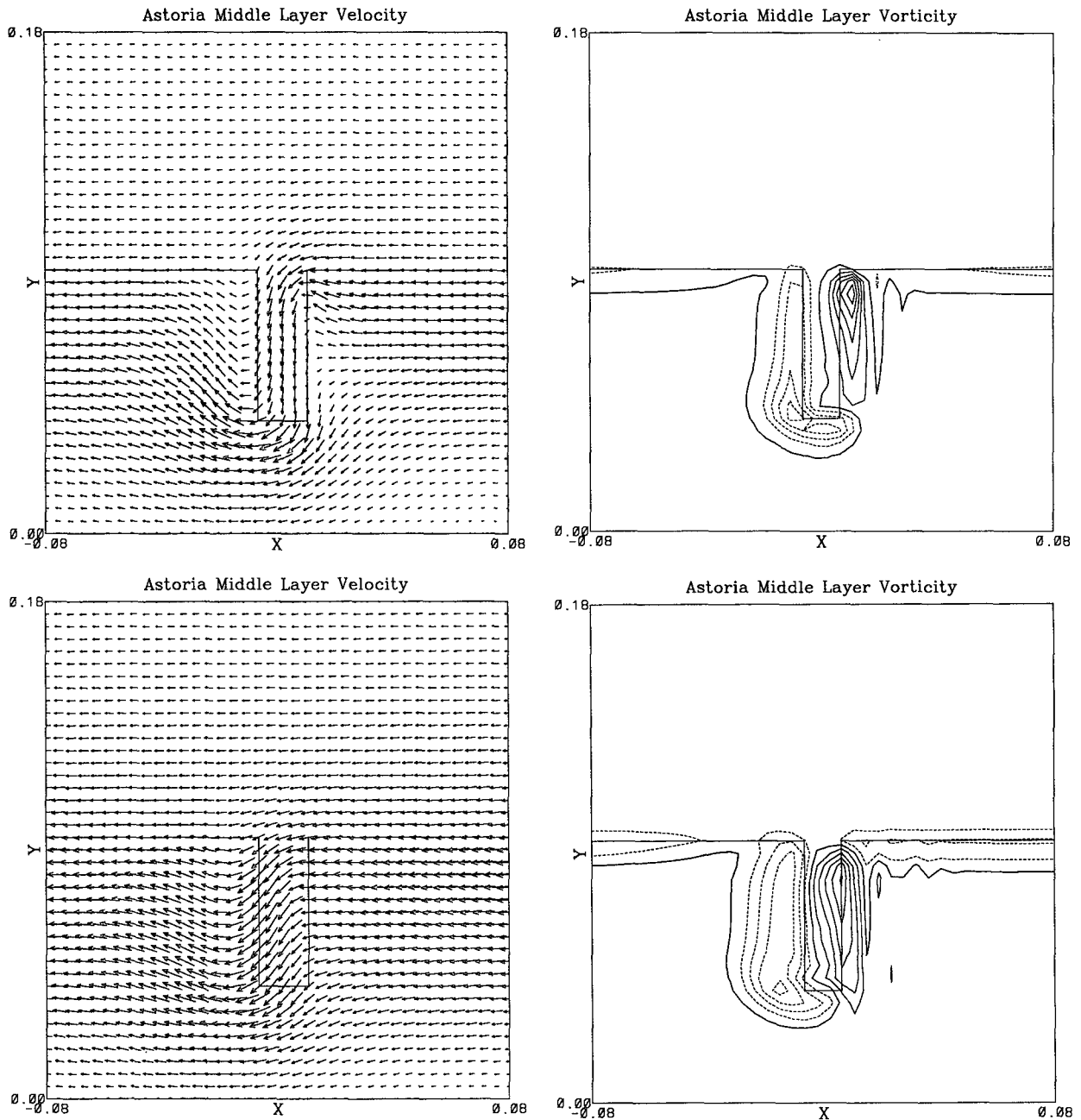
Astoria Middle Layer Vorticity

FIG. 13. Results after 24 hours for the nonlinear, stratified numerical model (run Astoria) over Astoria topography (see Table 2) with the following variations: Lower interface level moved down by 65 m (run A4). (a) The middle-layer velocity, maximum velocity vector is 16 cm s^{-1}. (b) The middle-layer vorticity, contoured from $-0.62f$ to $0.78f$ by $0.16f$. Increase in forcing by a factor of 2 (run A7). (c) The middle-layer velocity, maximum velocity vector is 23 cm s^{-1}. (d) The middle-layer vorticity, contoured from $-0.5f$ to $0.6f$ by $0.12f$.

geometry, the effect of varying the reduced gravities, the levels of the two interfaces, the shape of the bottom of the canyon, the strength and the position of the forcing will be considered. There are a large number of nondimensional numbers that can be formed from these and the other parameters of the system. Varying the parameters one at a time illustrates the dominance of

three of these numbers. Generally, the flow pattern is very robust to parameter variations. Table 3 gives the varied parameters, the nondimensional number that governs the field changes observed, and which of the fields actually changed.

The results indicate that only changes in the canyon depth effect the surface or upper interfaces. No change
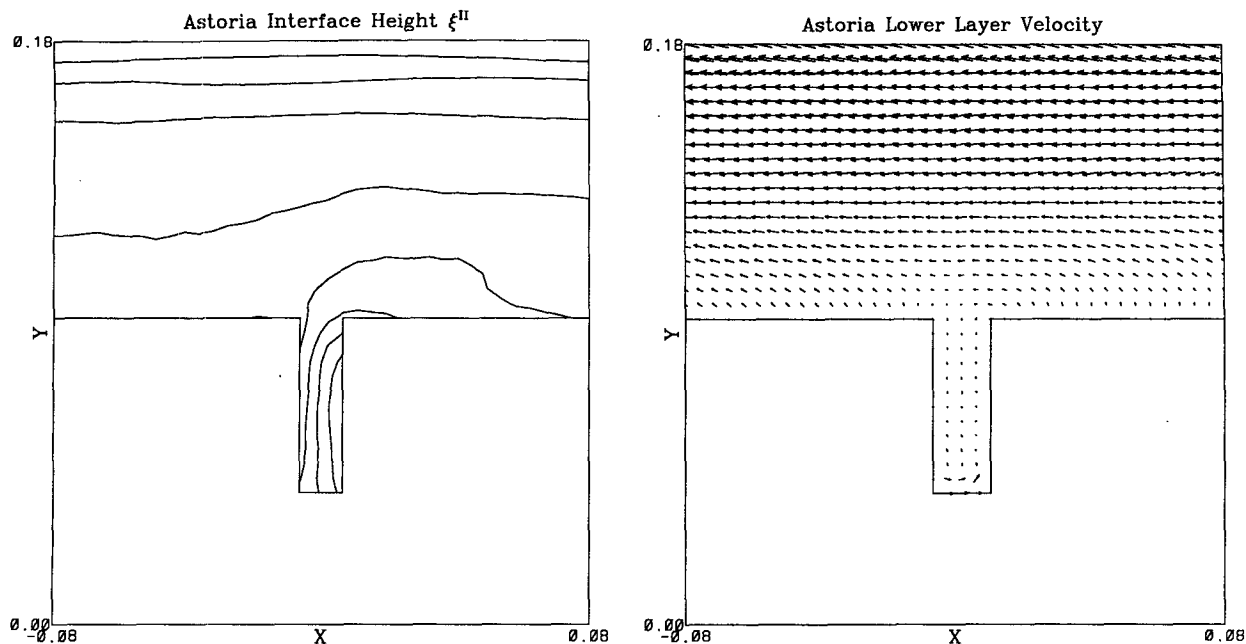
FIG. 14. Results after 24 hours for the nonlinear, stratified numerical model (run Astoria) over Astoria topography (see Table 2) but with the reduced gravity across lower interface increased by a factor of 5 (run A2). (a) The lower interface elevation, contoured from 0.8 m to 3.6 m by 0.4 m. (b) The lower-layer velocity, maximum velocity vector is 0.9 cm s^{-1}.

was observed in the surface velocity. If the forcing was more gradual, the surface velocities would deviate over the canyon as discussed in section 6b.

The middle-layer flow pattern is effected by two factors: its change in depth over the canyon and changes in the background flow speed. If the change in depth of the middle layer over the canyon is larger, the canyon has more effect on the flow and flow is diverted to flow more parallel to the canyon walls, as shown in Fig. 13. The region of strong anticyclonic vorticity is advected downstream by the middle-layer flow. Thus, if the background (no canyon) flow is increased, the anticyclonic vorticity moves farther downstream as shown in Fig. 13.

The amount of upwelling, that is, the height of the lower interface is primarily effected by the ratio of the pressure gradient along the canyon (given by the middle-layer velocity over the canyon, $\bar{u}_2$ divided by f) to the reduced gravity across this interface. If the flow is more along the canyon in the middle layer (less depth change in middle layer), the pressure gradient is reduced and so is the interface height as shown in Fig. 14. When the position of the forcing is moved, the final middle-layer velocities are similar but the interface height reflects, to some extent, the differences in the velocities at early times.

The velocity into the canyon in the lowest layer is affected by the pressure gradient along the canyon in the same way as the lower interface and by the speed of the baroclinic Kelvin wave. The baroclinic Kelvin

wave propagates from the head of the canyon, down the upstream side of the canyon, reversing the velocity to out canyon. A flat bottom increases the wave speed and, therefore, the distance from the head of the canyon over which the velocity has reversed at a given time as shown in Fig. 15.

e. Tully Canyon

A canyon loosely representing the geometry of Tully Canyon, a spur of Juan de Fuca Canyon, was run to investigate the long term, frictionally dominated solution. The fluid was assumed barotropic; the nonlinear terms were included. The canyon is 45 km long, 8 km wide, and cuts into a 90-km shelf. The canyon is 250 m deep and cuts through a shelf 100 m deep. The bends of the real canyon and the presence of the main canyon were not modeled.

The flow pattern is shown in Fig. 16a after almost 9 days, for which it has been stable for the last 3. The incoming flow splits near the head of the canyon, part going around the head of the canyon as predicted by the linear model but most going over the canyon wall close to the shelf break and up through the mouth of the canyon. The vorticity around the mouth of the canyon is strongly cyclonic (Fig. 16b). The flow within the canyon crosses the downstream edge of the canyon along its whole length (Fig. 16a). The flow downstream of the canyon is weakly anticyclonic (Fig. 16b).

The vorticity pattern, given the flow pattern, is easy to explain. Columns of fluid are stretched as they cross

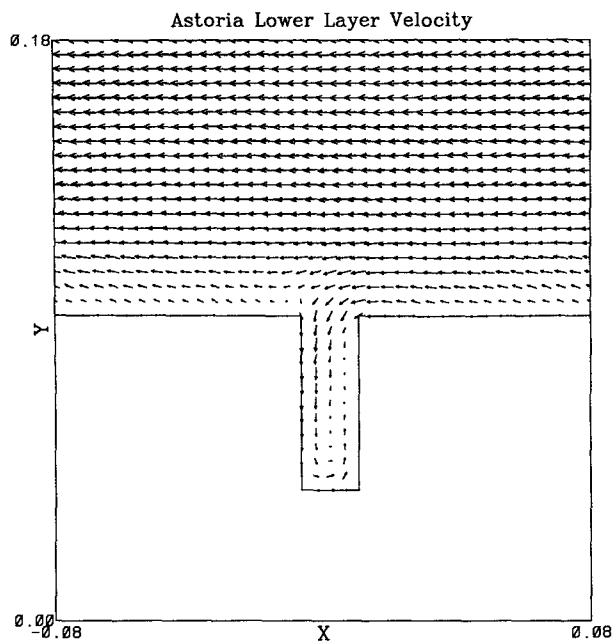## Astoria Lower Layer Velocity

FIG. 15. Results after 24 hours for the nonlinear, stratified numerical model (run Astoria) over Astoria topography (see Table 2) but with a flat bottom in the canyon (run A5). (a) The lower-layer velocity, maximum velocity vector is 1.4 cm s^{-1}.

canyon and so still have, approximately, their original potential vorticity as they cross back onto the shelf. The columns of fluid originally in the canyon have lost their potential vorticity signature due to spin down.

Observations consistently show that the Juan de Fuca eddy is cyclonic. The model predicts a strong cyclonic feature upstream and over the canyon, which implies that the eddy we observe over the small Tully Canyon is quite possibly due to the large main canyon downstream. However, the model does not predict the observed closed streamlines. A more complete analysis of a semi-infinite but finite width canyon, which better represents the geometry of the main canyon than the analytic work in this paper, can be found in Chen and Allen (1996).

Freeland and Denman (1982: Fig. 9) observed a strong shear between 50 m and 100 m, which the barotropic model cannot imitate. As well, the geometry of the canyon system with the presence of the Olympic Peninsula must strongly affect the flow. The model run is probably too nonlinear, with strong, 75 cm s^{-1} flows at all depths as opposed to the observations of weak flow at depth. In many ways, the linear, stratified run 2 (Fig. 9) is more consistent with the observations. The interface height η_1 (Fig. 9g) compares quite well with the dynamic height at 50 m relative to 100 m in September 1980 (Freeland and Denman 1982: Fig. 9). Note that the patterns should directly compare but there is a sign shift. The observed low in dynamic height over the canyon corresponds to the high interface height. However, run 2 has a small margin width and a long

the upstream side of the canyon, which leads to strongly cyclonic flow. Friction tends to spin down the vorticity, but the columns move quickly through the
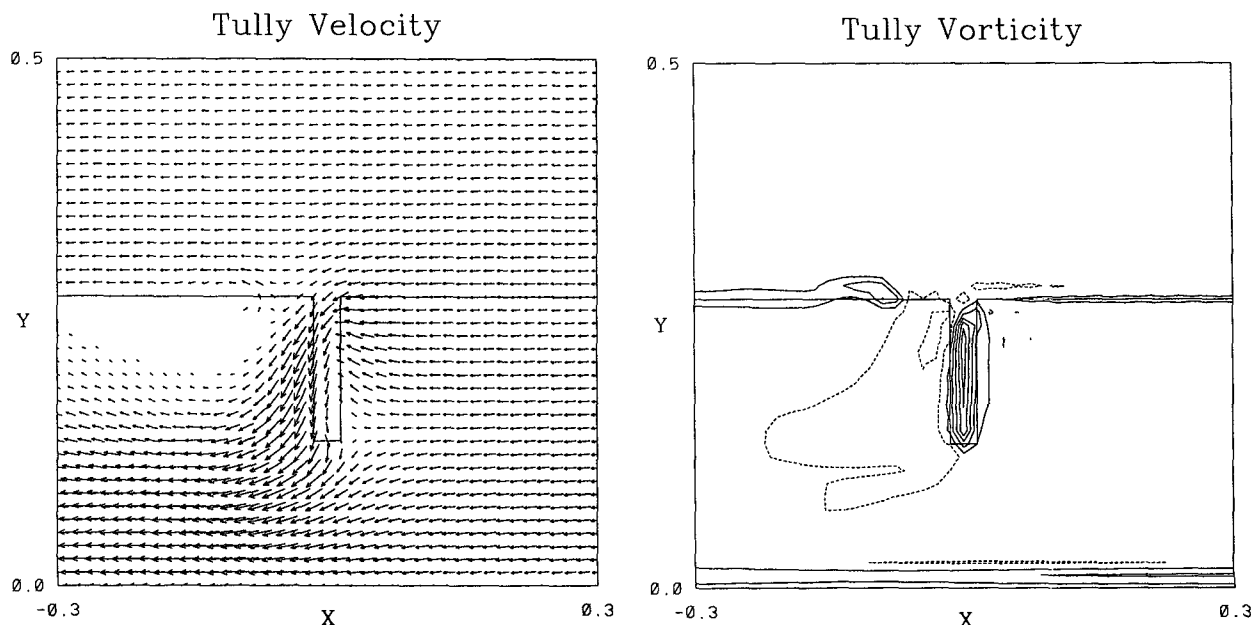
Tully Velocity

Tully Vorticity

FIG. 16. Results after 9 days for the nonlinear, homogeneous numerical model with bottom friction (run Tully). (a) The velocity, maximum velocity vector is 91 cm s^{-1}. (b) The vorticity, contoured from $-0.12f$ to $0.36f$ by $0.08f$.

canyon length, which probably explains the steep contours along the wall as opposed to the observations with steep contours toward the mouth of the canyon.

Wind forcing is not the only mechanism at work causing upwelling through Juan de Fuca Canyon. Weaver and Hsieh (1987) proposed that the estuarine flow of brackish water out of Juan de Fuca Strait causes the movement of deep water through the canyon as a deep return flow. The Eulerian velocities due to tidal rectification in this area will also contribute slightly to the cyclonic flow. Foreman et al. (1992) have recently calculated these velocities and find a weak, 1 to 2 cm s^{-1} cyclonic eddy in this region.

7. Summary

The tendency of a canyon to cause strong flows toward shore during upwelling favorable winds has been explained by two conceptually simple linear analytic models. The first model describes the process over a one-half to two day timescale (acceleration phase), whereas the second model describes longer timescales (steady phase). During the acceleration phase, in the linear regime:

1) The growing velocity in the layer in contact with the topography cannot cross the topography and travels around the head of the canyon, returning to its original distance from the coast.

2) Anticyclonic vorticity is generated in a homogeneous fluid and in the upper layers of a stratified fluid. Cyclonic vorticity is generated in the layer trapped within the canyon.

3) For a homogeneous fluid, upcanyon flow is of order 10 times stronger than flow across the shelf break. For a stratified fluid this increases to 50 times.

The comparison with the numerical models shows that the approximations (of an infinitesimally thin canyon with vertical walls and linear flow) produce a similar pattern to that predicted by the full nonlinear model. In the acceleration phase, modifications due to nonlinearity include:

1) The growing velocity in the layer in contact with the topography can cross the canyon walls. For a short canyon (less than the width of the shelf current) the flow tends to go around both ends of the canyon and not just around the head. The flow around the mouth of the canyon tends to flow up the canyon.

2) In the upper layers or in a homogeneous fluid anticyclonic flow is generated at the head of the canyon. In the layer in contact with the topography anticyclonic vorticity is generated along the downstream edge of the canyon and cyclonic vorticity along the upstream edge. The layer trapped within the canyon is cyclonic.

3) The upcanyon flow is greatly increased in the upper layers (over that in the linear case) due to the

movement of the flow pattern downstream. The shoreward branch of the shelf current lies over the canyon.

In the steady phase:

1) The linear theory predicts poorly the nonlinear numerical results.

2) The strongest vorticity is cyclonic and lies over the canyon or slightly upstream. Anticyclonic vorticity is reduced by the bottom friction over the shelf.

Upcanyon flow is caused by:

1) The inshore branch of the main flow that lies over the canyon due to nonlinear effects (the flow turns inshore due to cyclonic vorticity being generated as the fluid columns move over the canyon).

2) The divergence of the steady flow feeds the growing shelf current or in the steady case, the convergence of the bottom Ekman layer.

Numerical models approximating Astoria and Tully Canyons allowed the theory to be compared to observations. For Astoria Canyon, many of the qualitative features are in agreement. The agreement for Tully Canyon is much poorer, perhaps due to the complicated topography/geometry. A full test of the theory will require more realistic topography and stratification.

APPENDIX

Solutions over Rectilinear Shelves

a. Solution for barotropic Rossby adjustment over a shelf

Consider the solution of (9) over a topography:

$$H = \begin{cases} H_S, & y < S \\ H_D, & y > S, \end{cases} \qquad (A1)$$

with q as given in (2). Assuming that as the forcing and the topography are independent of x the solution will be: (9) becomes, dropping the subscript 1,

$$\frac{gh}{f^2}\frac{\partial^2 \eta}{\partial y^2} - \eta = \frac{q}{f}. \qquad (A2)$$

The boundary conditions are

$$\partial\eta/\partial y = 0 \quad \text{at} \quad y = 0 \quad (\text{see section 2}),$$

$$\eta, \partial\eta/\partial y \quad \text{continuous at} \quad y = E,$$

$\eta, h\partial\eta/\partial y$ are continuous at $y = S$ (as hv_0 must be continuous and $v_0 \propto u_1 \propto \partial\eta/\partial y$),

$$\eta \to 0 \quad \text{as} \quad y \to \infty. \tag{A3}$$

Thus, solutions in the various domains are exponentials. Combined with the four boundary conditions at $y = E$ and $y = S$ results in four linear equations that can be solved by elimination. The solution is

$$\eta = \frac{q_0}{f} \left(\frac{\alpha \sinh[(S-E)/a_s] + \cosh[(S-E)/a_s]}{\alpha \sinh(S/a_s) + \cosh(S/a_s)} \right)$$

$$\times \cosh(y/a_s) - \frac{q_0}{f}, \quad y < E,$$

$$\eta = -\frac{q_0}{f} \left(\frac{\sinh(E/a_s)}{\alpha \sinh(S/a_s) + \cosh(S/a_s)} \right)$$

$$\times \{\alpha \cosh[(S-y)]/a_s$$

$$+ \sinh[(S-y)/a_s]\}, \quad E < y < S,$$

$$\eta = -\frac{q_0}{f} \left(\frac{\sinh(E/a_s)}{\alpha \sinh(S/a_s) + \cosh(S/a_s)} \right)$$

$$\times \exp(-(y-S)/a_d), \quad y > S, \tag{A4}$$

where $\alpha^2 = H_S/H_D$, and where a_s (a_d) is the Rossby radius over (off) the shelf.

The height at the shelf break is given by

$$\eta = -\frac{q_0}{f} \sinh(E/a_s)$$

$$\times \exp(-S/a_s) \left(\frac{\alpha \exp(S/a_s)}{\alpha \sinh(S/a_s) + \cosh(S/a_s)} \right)$$

$$= -\sigma \frac{q_0}{f} \sinh(E/a_s) \exp(-S/a_s). \tag{A5}$$

The last fraction, σ, reduces to $2/(1 + \sqrt{H_D/H_S})$ for S/a_s not very small. For the model canyon with $S = 2a_s$ and $H_S/H_D = 1/8$, $\sigma = 0.5179$. We have assumed η_0 is zero, which is justified as there is nothing to force η_0 at the shelf break.

b. Diffusion solution over a shelf

Consider the solution of (42) over a topography (A1) with q as given in (2). Assuming that as the forcing and the topography are independent of x, the solution will be independent of x, (42) becomes $\partial^2\eta/\partial y^2 = 0$, and $v = 0$.

The boundary condition at $y = E$ is that the flux perpendicular to the coast in the lower Ekman layer and in the main fluid must equal the flux in the upper Ekman layer. As $v = 0$ the flux is merely in the Ekman layers. The lower-layer Ekman flux depends on the velocity u, and thus $u = -2qE/\delta$ at $y = E$. At $y = S$, the flux must be continuous, which implies that $hv - u\delta/2$ is continuous.

The solution allowing u to remain finite far from the coast is

$$\eta = \eta_w + \frac{2qfEy}{g\delta} \tag{A6a}$$

$$u = \frac{-2qE}{\delta}, \tag{A6b}$$

where η_w is the height at the coast.

c. Rossby adjustment over a shelf for a three-layer fluid

The solution for baroclinic Rossby adjustment for a layered fluid follows the method used in the homogeneous case. For the case of three layers where the deep layer exists only off the shelf, there are two Rossby radii on the shelf and three off the shelf. Imposing the boundary conditions of no growing flow at the wall (because there was none to start with) and of boundedness as $y \to \infty$ leaves a set of solutions for the three layers with a total of 21 constants. The following boundary conditions were imposed.

At $y = E$:

- continuity of pressure in both layers
- continuity of velocity in both layers
- continuity of the first derivative of velocity in both layers
- continuity of the second derivative of velocity in both layers

At $y = S$

- continuity of pressure in upper two layers
- continuity of flux $h(u_0, v_0)$ in upper two layers
- continuity of the first derivative of flux in upper two layers
- continuity of the second derivative of flux in upper two layers
- zero velocity into the shelf in the lowest layer
- zero derivative of velocity into the shelf in the lowest layer

Globally:

- Conservation of mass for each of the layers.

These 21 conditions allow the calculation of the 21 constants. The most straightforward way to solve for these constants is numerically on a case by case basis.

In the case considered here, the forcing is through the removal of upper-layer fluid near the coast. Thus, the barotropic mode is primarily forced and the upper-

layer and second-layer growing streamfunctions are very similar both to each other and the homogeneous case. The deepest layer has a jet against the shelf in the same direction as the flow in the other layers.

REFERENCES

Abramowitz, M., and I. A. Stegun, 1972: *Handbook of Mathematical Functions.* Dover, 1046 pp.

Allen, J. S., 1992: The effects of alongshore variations in bottom topography on coastal upwelling (abstract). *Eos, Trans. Amer. Geophys. Union,* **73**(Suppl), 317.

Allen, S. E., 1988: Rossby adjustment over a slope. Ph.D. thesis, University of Cambridge, 206 pp.

Arakawa, A., and V. R. Lamb, 1981: A potential enstrophy and energy conserving scheme for the shallow water equations. *Mon. Wea. Rev.,* **109**, 18–36.

Butman, B., 1983: Long term current measurements in Lydonia and Oceanographer Canyons. *Eos, Trans. Amer. Geophys. Union,* **64**, 1050–1051.

Chen, X., and S. E. Allen, 1996: Influence of canyons on shelf currents—a theoretical study. *J. Geophys. Res.,* in press.

Fang, W., and W. W. Hsieh, 1993: Summer sea surface temperature variability off Vancouver Island from satellite data. *J. Geophys. Res.,* **98**, 14 391–14 300.

Foreman, M. G. G., A. M. Bapista, and R. A. Walters, 1992: Tidal model studies of particle trajectories around a shallow coastal bank. *Atmos.–Ocean,* **30**, 43–69.

Freeland, H. J., and K. L. Denman, 1982: A topographically controlled upwelling center off southern Vancouver Island. *J. Mar. Res.,* **40**, 1069–1093.

Gill, A. E., M. K. Davey, E. R. Johnson, and P. F. Linden, 1986: Rossby adjustment over a step. *J. Mar. Res.,* **44**, 713–738.

Hickey, B. M., 1987: Patterns and processes of circulation over the Washington continental shelf and slope. *Coastal Oceanography of Washington and Oregon,* Vol. 47, *Elsevier Oceanography Series,* M. R. Landry and B. M. Hickey, Eds. Elsevier, 41–115.

——, E. Baker, and N. Kachel, 1986: Suspended particle movement in and around Quinault submarine canyon. *Mar. Geol.,* **71**, 35–83.

Hotchkiss, F. S., and C. Wunsch, 1982: Internal waves in Hudson Canyon with possible geological implications. *Deep-Sea Res.,* **29**, 415–442.

Klinck, J. M., 1988: The influence of a narrow transverse canyon on initially geostrophic flow. *J. Geophys. Res.,* **93C**, 509–515.

——, 1989: Geostrophic adjustment over submarine canyons. *J. Geophys. Res.,* **94C**, 6133–6144.

Ma, H., 1992: A simple model for upwelling through Moresby Trough. M.S. thesis, Department of Oceanography, University of British Columbia, 82 pp.

Mackas, D. L., and H. A. Sefton, 1982: Plankton species assemblages off southern Vancouver Island: Geographic pattern and temporal variability. *J. Mar. Res.,* **40**, 1173–1200.

Mcdonald, N. R., and J. Imberger, 1992: Withdrawal of a stratified fluid from a rotating channel. *J. Fluid Mech.,* **235**, 643–664.

Monismith, S. G., and T. Maxworthy, 1989: Selective withdrawal and spin-up of a rotating stratified fluid. *J. Fluid Mech.,* **199**, 377–401.

Naasse, D. L., and A. Kabbaj, 1990: Détermination des perturbations locales en théorie de l'eau peu profonde généralisée. Problème d'Hilbert-Riemann. *Oceanol. Acta,* **13**, 171–176.

Pedlosky, J., 1974: Longshore currents, upwelling and bottom topography. *J. Phys. Oceanogr.,* **4**, 214–226.

Weaver, A. J., and W. W. Hsieh, 1987: The influence of buoyancy flux from estuaries on continental shelf circulation. *J. Phys. Oceanogr.,* **17**, 2127–2140.